Lawrence Berkeley Laboratory
UNIVERSITY OF CALIFORNIA

Materials & Molecular Research Division

POWDER METALLURGY PROCESSED A15 Nb_3Al SUPERCONDUCTING WIRES

J. Minghuang Hong
(M.S. thesis)

June 1982

Prepared for the U.S. Department of Energy under Contract DE-AC03-76SF00098

DISCLAIMER

LBL-14749

POWDER METALLURGY PROCESSED A15 Nb_3Al SUPERCONDUCTING WIRES

J. Minghuang Hong

M.S. Thesis

June 1982

Materials and Molecular Research Division
Lawrence Berkeley Laboratory
University of California
Berkeley, CA 94720

This work was supported by the Division of Materials Science, Office of Basic Energy Sciences of the U.S. Department of Energy under Contract Number DE-AC03-76SF00098.

To my parents

ACKNOWLEDGEMENTS

I would like to thank my advisor, Professor J. W. Morris, Jr., for his encouragement and support throughout this thesis work and for his providing me the free research atmosphere in which I enjoyed very much.

I also thank the members in this research group for many helpful discussions, in particular, Dan Dietderich and I-Wei Wu, who in the the early stage of this thesis work helped me establish some of the experimental techniques employed. I am grateful to Gee-Min Chang, who is also a group member, and to Peggy Y. Hou, who is in the same department, for the discussions, suggestions and helps in many respects.

It was an unforgetable experience to work with Mr. J. T. Holthuis in Materials and Molecular Research Division of Lawrence Berkeley Laboratory, whose delicate hands and thoughtful mind have solved many problems in the sample preparation and made this work possible. His help is well appreciated.

My greatest appreciatons goes to Dr. Minghwei Hong , who is now working at Bell Laboratories, Murray Hill, for his introducing me to this research topic and for his guidence and many helpful discussions in leading me to understand the superconductivity of the A15 materials. His dedication, keen sights, and delicacy in performing scientific research are also respected.

I am deeply in debt to my parents and to all the other members in the family for their tremendous support and understanding through all these years , which have been a very strong and important source to my momentum.

I would like to express my gratitude to Min-Chi Tsai, who is about

to accomplish her Ph. D. degree in Chemistry Department, for the helps and discussions in preparing this manuscript as well as many other respects, and to Dr. J. Kwo of Bell Laboratories, Murray Hill for her helps and encouragement.

I would like to express my appreciation to those people who contributed to the critical current density measurements of this work : Dr. M. Hong , Mr. J. T. Holthuis , D. Dietderich , I. W. Wu , and W. Hassenzahl of Accelerator and Fusion Research Division.

Finally , I wish to thank Professor J. W. Morris, Jr. , Drs. D. P. Whittle, and R. Gronsky for reading and correcting this manuscript.

This work was supported by the Division of Materials Science, Office of Basic Energy Sciences of the U.S. Department of Energy under Contract Number DE-AC03-76SF00098.

TABLE OF CONTENT

I. Introduction..... 1

II. Experimental procedure..... 6

A. Preparation of powders..... 6

B. Mechanical deformation.....13

C. Heat treatments.....18

D. Superconducting properties measurements.....18

E. Materials characterization.....19

III. Results and discussion.....23

A. Metallurgical characteristics.....23

A.1. Preferred orientation and configuration of the unreacted wire.....23

A.2. The phases present.....31

A.3. Microstructure and morphology.....34

B. Control and optimization of T_c and overall J_c by heat treatments.....51

B.1. T_c and single temperature heat treatments.....52

B.2. T_c and multiple-step heat treatments.....57

B.3. Overall J_c and heat treatments.....61

C. Influence on overall J_c of powder preparation and deformation process.....78

C.1. Al content.....81

C.2. Areal reduction ratio.....85

D. Further discussion.....93

IV. Conclusions.....99

V. References.....101

POWDER METALLURGY PROCESSED A15 Nb_3Al SUPERCONDUCTING WIRES

By

Master of Science in Engineering Science

J. Minghuang Hong

Department of Materials Science and Mineral Engineering

J. W. Morris, Jr.
Chairman of Commitee

ABSTRACT

The possibility of the manufacture of superconducting A15 Nb_3Al wires by a powder metallurgy process was explored. A T_c value of 17 K and overall J_c value of $> 10^4$ A/cm^2 at 15 teslas and 4.2 K were obtained. The variations of both T_c and overall J_c with the temperature and time of the heat treatment employed were investigated. Based on those, a multiple-step heat treatment was proposed and found to be beneficial to both T_c and overall J_c. It is believed that this resulted from the improvement of the superconducting characteristics within the wire. The variations of the overall J_c with other processing parameters were also investigated. They are the reduction in the transverse cross section, powder size, powder size ratio, and Al content. An increase of Al content from 3 to 4 wt % Al resulted in an increase of > 50% of the overall critical current density. However, a further increase by 1 wt% Al neither improved nor degraded the overall J_c of the powder wire. The reduction in the transverse cross

section was found to have a significant influence on overall J_c. The measured critical current density increased monotonically with the reduction and was still increasing even for a reduction as large as 99.994%. Based on the results obtained, the importance of the filament thickness of Nb and Al and the Nb-Al interfacial area in determining the critical current density was discussed. Preliminary characterization of the microstucture of the reacted layer within the powder wire was performed using a transmission electron microscope and the result was presented.

CHAPTER I. INTRODUCTION

The superconducting materials which show the greatest promise for the windings of high-field superconducting magnets are intermetallic compounds of stoichiometric composition A_3B with the A15 crystal structure. These A15 compounds include the superconducting phases of Nb_3Sn, V_3Ga, V_3Si, Nb_3Al, Nb_3Ga, Nb_3Ge, and ternary $Nb_3(Al_{0.8}Ge_{0.2})$. They combine high critical temperature (T_c) with high upper critical field (H_{c2}) and high current density (J_c). Values of T_c and H_{c2} at 0 K for these phases are listed in Table I-1. For comparison, those of the superconducting bcc alloy Nb-Ti, which is extensively employed in constructing magnets to be used at fields of < 8 teslas, are also included. Though they possess much better superconducting properties, the A15 compounds are brittle intermetallic phases. They are therefore difficult to form into long lengths of superconducting wires as required for use in high-field magnet windings.

In the case of Nb_3Sn and V_3Ga, this manufacturing difficulty has been largely overcome by the development of the "Bronze"[1,2] and "In-Situ" processes[3-8], which utilize the solid-state reaction between Nb or V and Sn or Ga dissolved in Cu. In these processes, continuous filaments of Nb or V are inserted or formed "in-situ" within a suitable matrix. The filaments and matrix are subsequently coextruded into a fine wire. Wires thus processed can be bundled together to form a tape. The A15 compound is then formed at the filament-matrix interface through a reaction which extracts the Sn or Ga from the matrix. These processes have been successfully employed for the manufacturing of high - field superconducting wires containing multifilamentary Nb_3Sn or

Table I-1. Superconducting Properties of Promising A15 Compounds

A15 Compounds	T_c (K)	H_{c2}^* (T)
Nb_3Sn	18.3	30.0
V_3Ga	15.4	35.0
V_3Si	17.0	34.0
Nb_3Al	19.1	33.0
Nb_3Ga	20.3	34.0
Nb_3Ge	23.0	37.0
$Nb_3(Al_{0.8}Ge_{0.2})$	20.7	44.5

* Extrapolated to 0 K.

V_3Ga for magnet windings. They are, however, inapplicable for thermodynamic reasons to the manufacture of wires containing such A15 compounds as Nb_3Al or Nb_3Ge which have better inherent superconducting properties.[9]

Because of the inapplicability of the "Bronze" and "In-situ" processes, manufacturing research on wires based on the other promising A15 compounds has concentrated on the establishment of a fine admixture of the primary constituents and the subsequent formation of the A15 phase through some direct reaction processes after the wire is drawn. At least four distinct manufacturing processes have been explored. These include:

(1) The "powder metallurgy process", in which a mixture of powders of the primary constituents is extruded into a wire before reaction. This process has been utilized in the manufacture of the Nb_3Al[10,11] and Nb_3Sn superconducting wires.[12,13] Comparable critical current densities of $\sim 10^4$ A/cm^2 at 15 T were reported for both systems.[10,12] In the case of the Nb_3Sn system, Sn can be incorporated through the external or internal diffusion method.

(2) The "jelly-roll or swiss-roll process", in which thin foils of the two constituents are superimposed and tightly wound around a copper cylinder and then extruded for subsequent reactions.[14] A critical current density of $\sim 10^5$ A/cm^2 at 6.4 T and 4.2 K was achieved. This process was later modified and applied to the Nb-Sn system, in which thin meshed Nb foils were employed.[15]

(3) The "infiltration process", in which a porous compact of the refractory constituent is sintered , liquid - infiltrated by the other constituent, and subsequently drawn into a fine wire for

reaction.[16]

(4) The "direct solid-state precipitation proccess", in which a supersaturated solid solution of B in A is mechanically deformed into a fine wire or a tape and the A15 A_3B compound is subsequently formed by a precipitation reaction at elevated temperatures.[17,18] The Nb_3Al wire thus proccessed could have a critical current density of $\sim 10^4$ A/cm^2 at 14 T and 4.2 K.

The first of these, the "powder metallurgy" approach, offers the advantages of an appealingly simple, flexible, and potentially economical manufacturing process. In this approach, the powder size, powder size ratio(s), and chemical composition can be varied with ease. The mechanical deformation required is, in general, low and straightforward as compared with, e.g., the commercialized "Bronze" process. No intermediate annealing was necessary in this study.

Nb_3Al, first synthesized in the A15 crystal structure and found to have a T_c of 17.5 K,[19,20] has long been interested not only because of its good superconducting properties[21-24] but also its controversies in the higher temperature homogeneity range[25-27] and electronic band structure.[28-32] The T_c value was later raised to 18.8 K using a variety of heat treatments.[21] The H_{c2} value at 0 K was found to be over 30 T,[22] and J_c was recently reported to have a value as high as 10^5 A/cm^2 near 20 T at 4.2 K.[23,24] Unlike well-ordered, stoichiometric compounds such as Nb_3Sn and V_3Si, Nb_3Al does not exhibit a high density of states at the Fermi level either by heat capacity[21,28] or magnetic susceptibility measurements.[21,29] A high density of states at the Fermi level is believed to play an important role in the favorable occurrence of high-T_c superconductivity in the conventional model.[30]

Recent analyses by both superconducting tunneling[31] and critical field measurements[32] on Nb-Al thin films, however, suggested that the phonon-mode softening might be a more important factor. In spite of these controversies, many methods have been developed to fabricate practical Nb_3Al superconductors due to its excellent superconducting properties.[10,11,14,17,18,33-37]

In this thesis, the results of the developmental research on powder- metallurgy - processed A15 Nb_3Al superconducting wires are presented. The fabrication of a good superconducting wire requires the control of at least two distinct aspects of the A15 phase: its internal composition and state of order, which determine its inherent superconducting characteristics, and its microstructural distribution within the wire, including such factors as its volume fraction, grain size, and continuity, which determine the peak critical current a phase of given internal state can transport. The body of this thesis consists of two chapters. The experimental procedure employed is described in the next chapter. It includes the details of the powder metallurgy process, the superconducting property measurements, and methods utilized to study the metallurgical characteristics of the product wires. Chapter III concentrates on the characterization of metallurgical characteristics of powder-metallurgy-processed wires and modification of processing to improve the microstructure and to enhance the inherent superconducting characteristics of the A15 phase. A discussion on the importance of the thickness of Nb and Al filaments and the Nb - Al interfacial area in the unreacted wire is presented at the end of Chapter III.

CHAPTER II. EXPERIMENTAL PROCEDURE

The powder metallurgy (P/M) approach is a series of simple and straightforward processes, which begins with powder preparation, then mechanical deformation, and the introduction of the A15 phase through heat treatments (Figure II-1). The powder preparation includes choosing the powders and Al content, dehydrogenation of Nb hydride powders, and thorough mixing of the constituent powders. The mechanical deformation includes compacting, form-rolling, swaging, and wire-drawing. Heat treatments were performed at the temperature range of 700 - 1100°C. Neither the intermediate annealing nor the geometry consideration (except the size ratio(s) among constituent powders) is required. The material and processing characteristics for the samples used are outlined in Table II-1.

A. Preparation of Powders

High purity Al powders and Nb hydride powders[1] were first sized by screening through appropriate sieves.[2] Because the smallest opening of the sieves available was about 40 microns, a microparticle classifier[3] was used to obtain a finer sizing of the powders. These powders are shown in two scanning electron micrographs in Figure II-2. The Nb powders in Figure II-2a appear to be facet-like, which indicates the brittleness of powders introduced by the hydride process. This brittleness was used to obtain Nb powders of sizes < 50 microns by crushing powders of several hundred microns in size against steel beads. One of the advantages of employing this method, rather than

Figure II-1. Schematic description of the powder metallurgy approach employed in the manufacture the A15 Nb_3Al superconducting wires.

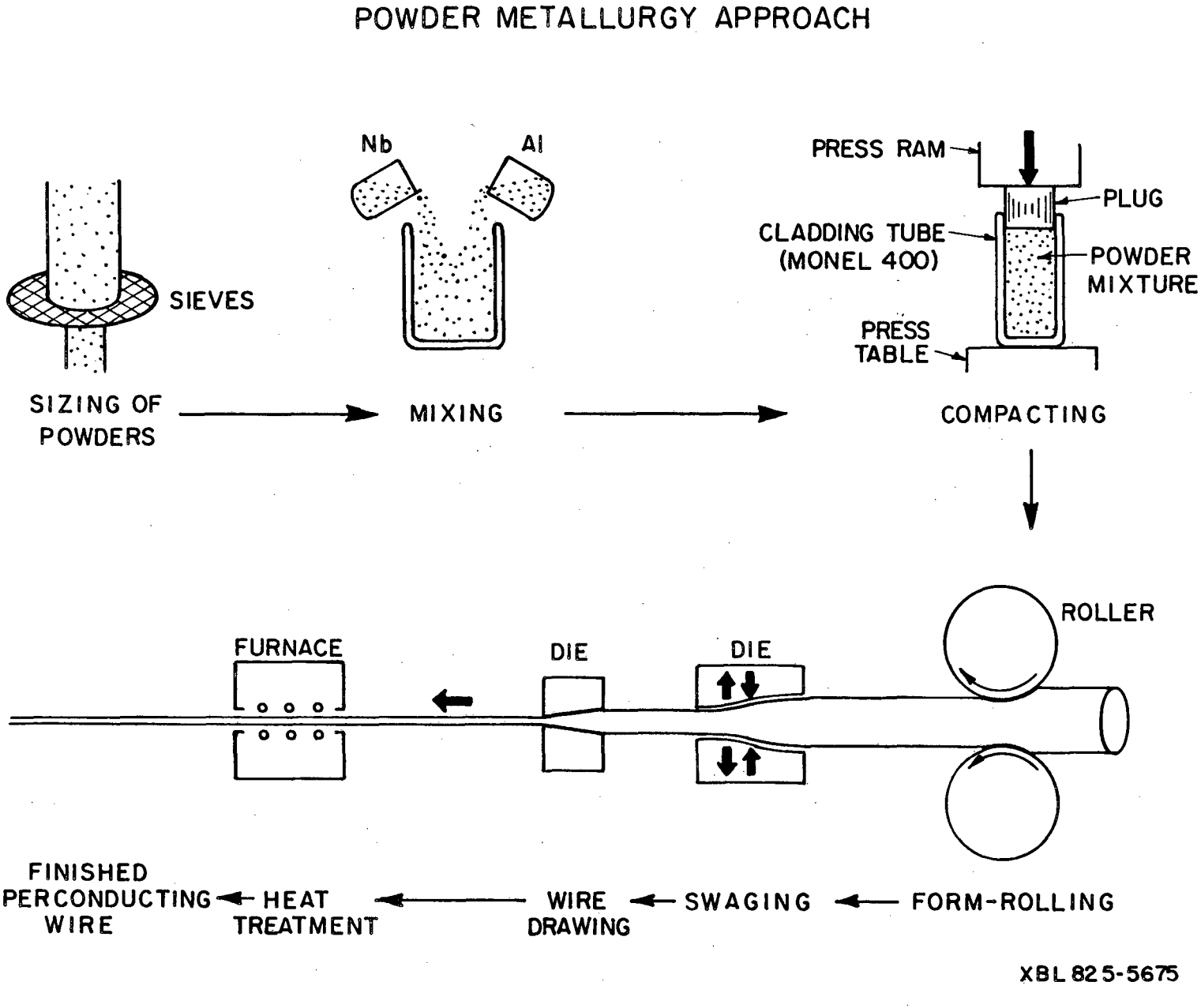
POWDER METALLURGY APPROACH
Nb
Al
SIEVES
PRESS RAM
PLUG
CLADDING TUBE
(MONEL 400)
POWDER
MIXTURE
PRESS
TABLE
SIZING OF
POWDERS
MIXING
COMPACTING
ROLLER
FURNACE
DIE
DIE
FINISHED
SUPERCONDUCTING
WIRE
HEAT
TREATMENT
WIRE
DRAWING
SWAGING
FORM-ROLLING
XBL 825-5675

Figure II-1

Table II-1. Sample Characteristics of Powder Metallurgy Processed Nb-Al Wires

Sample Number	Chemical Composion	Initial Powder Size (μm)		Areal Reduction Ratio	Diameter* (mm)
		Nb	Al		
80824	5 wt% Al	62-105	< 44	400	0.18
810422	3 wt% Al	< 37	< 10	1400	0.22
810608	4 wt% Al	~ 54	~ 20	7000	0.11
811027	5 wt% Al	~ 54	~ 20	630-17,700	0.11

* Excluding the cladding material.

Figure II-2. Scanning electron micrographs of the Nb and Al powders employed: (a) Nb hydride powders , manufactured by the hydrogenation of zone - refined Nb , are facet-like and have sharp edges. (b) Al powders, manufactured by the atomization process , are round and have smoother surfaces.

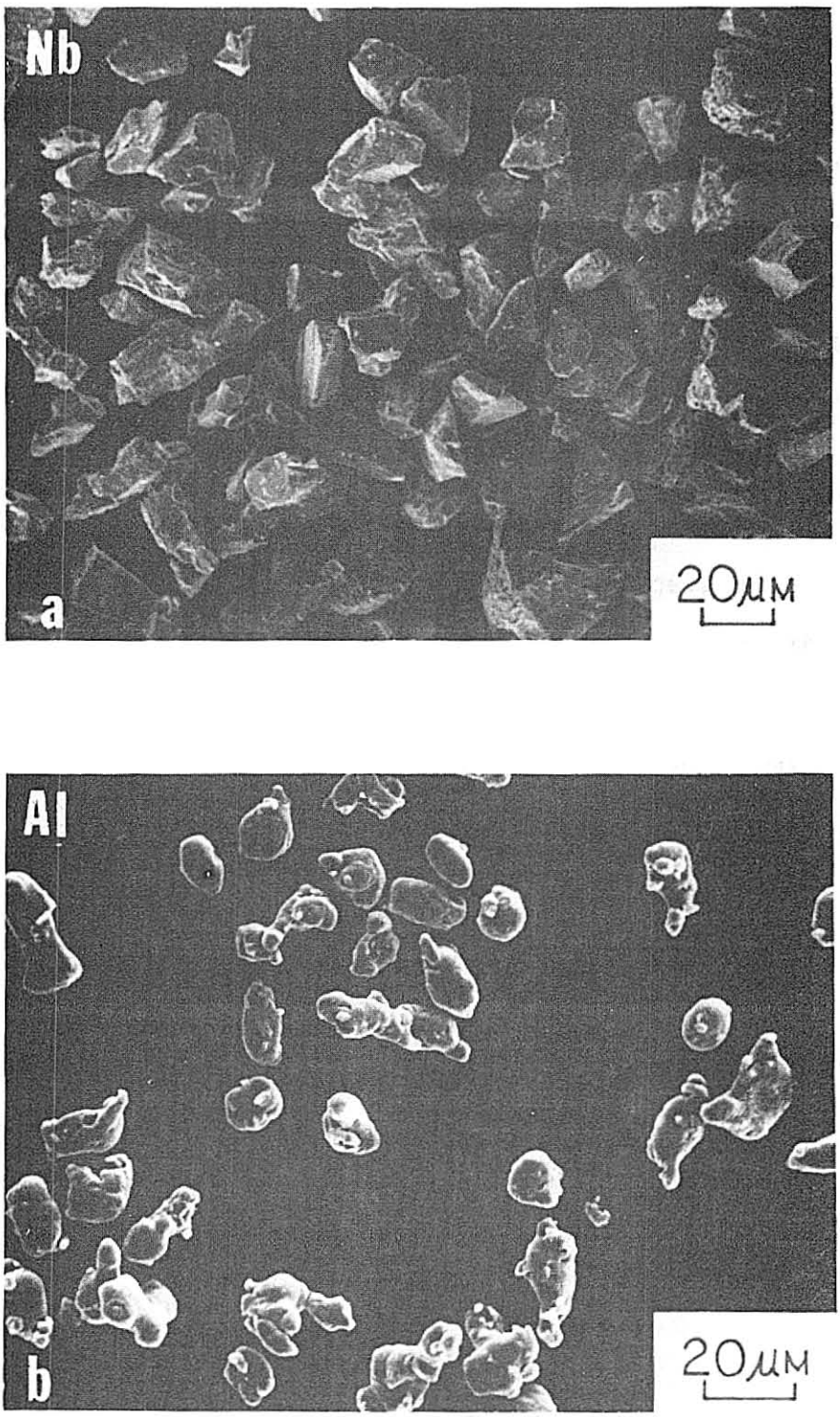

XBB 825-4405

Figure II-2

just using small powders manufactured by processes like atomization , is that the resultant powders would contain less impurities , e.g., oxygen and silicon. However, this method could not reduce the amount of tantalum present, which was typically on the order of 500 ppm . Impurities could be very crucial in determining the deformability of the powders, since it is known that even a small amount of impurities, especially interstitial type, would have a nontrivial contribution to the microhardness of powders.

Flukiger et al.[4] have used the same process to acquire the Nb powders. They also compared the properties of the Nb powders fabricated by different processes[4,5] and concluded that the zone - refined, hydride - dehydride - processed Nb powders gave the most satisfactory result. The Al powders , fabricated by the atomization process , as shown in Figure II-2b, have round shapes and smoother surfaces compared to Nb powders. It is noticed that the size distribution of Nb and Al powders are quite narrow, which justifies our method of sizing.

The Nb hydride powders are dehydrogenated by appropriate heat treatments. They were first put in a ceramic crucible and tightly covered with two tantalum nets . The opening of the nets was small enough to avoid Nb powders from " popping " out of the crucible during the heat treatment, yet still allowed the hydrogen gas produced to pass through. The crucible was then seated in a Brew furnace and the whole chamber was evacuated. When the pressure dropped to 10^{-6} - 10^{-7} torr, the temperature was increased to 700°C . The hydrogen gas produced would bring the pressure up to 10^{-2} - 10^{-3} torr initially. The process was considered to be completed after the pressure had reached 10^{-6} - 10^{-7} torr again and had a negligible increase if the temperature

were to be raised by 100°C for several minutes. This usually happened after an hour or so for a sample weighed about 100g.

After furnace - cooling to room temperature, the chamber was back-filled with argon gas , an inert gas heavier than air . The crucible was quickly transferred to a vacuum chamber in which Al powders of chosen weight and size were added to the now hydride - dehydride Nb powders. The powder mixture was then transferred into another bottle and filled with argon gas. The tightly closed bottle was machine-mixed for half an hour or so to achieve thorough mixing. Several inert beads were also enclosed to prevent Al powders from aggregating. Wires were made with three different Al contents: 5, 4 and 3 wt% (Table II-1).

B. Mechanical Deformation

After being thoroughly mixed, the powder mixture was compacted in a cladding material with a typical compressing stress of 35,000 psi. Several materials , including Cu , were used as cladding tubes. Monel 400 , a Ni-based alloy,[6] was found to have the most satisfactory performance. Limited by the apparatus available, the mechanical deformation processes employed were form-rolling , swaging , and wire-drawing, instead of extrusion . Since the roller handles square rods better than round rods , all of the cladding tubes were made in the following way: A commercial round Monel 400 rod (melting point of 1300 - 1350°C) was warm - rolled to become a square rod. A circular hole was drilled in the center along the longitudinal direction. A short piece of round rod , which was of the same material as the cladding tube and of

a diameter slightly (2 - 3 mils) larger than the hole drilled, was also machined to serve as a plug , which in turn served as a piston while compacting the powder mixture . Cladding tubes of various dimensions were used . The largest was 0.875 inch x 0.875 inch with a hole diameter of 0.568 inch . Before putting the powder mixture , these tubes were cleaned by immersing in acetone with microwave - aggitation, followed by etching for 30 seconds in a solution of HNO_3 : H_2O = 5 : 1, and then washed by alcohol, and blow-dried with hot air.

The cladding tube containing the compacted powder mixture , was processed by form - rolling to reduce the transverse cross section down to about 3/16 inch x 3/16 inch . This long square rod was then swaged to obtain a round shape with a diameter of about 0.100 inch in order to be conveniently drawn. The wire - drawing process was proved to be rather easy if the areal reduction ratio , R_o , defined as the ratio between the the tranverse cross sections before and after passing through the die, was no more than 1.10 . In other words, the reduction in tranverse cross section should be roughly within 10% . However, smaller reductions are preferred. Two kinds of dies were used: diamond and tungsten carbide. Though of better performance, the former is only available at small sizes.

The reduction of the powder mixture is usually slightly larger than that of the entire wire . It is meaningful , therefore , to define another parameter , R , as the ratio between the transverse cross sections of the powder mixture (instead of also taking the cladding into account as used to define R_o) before and after deformation. Significantly, an R value as high as 17,700 has been achieved. The improtance of R in affecting the superconducting properties will be discussed in

the following chapter . The deformation process described above also has two main effects on the powders themselves:

(1) Powders were elongated along the wire direction . The scanning electron micrographs in Figure II-3 , showing the wire configuration of an unreacted Nb 5 wt% Al (80824) wire , clearly illustrates this effect. Al and cladding materials have been etched away. The Nb powders , or more appropriately named , the Nb filaments , are all parallel to one another in the wire direction. Their average width is rather uniform throughout the wire examined , as illustrated in Figure II-3b , which justifies the chosen approach for deformation . In Figure II-3a , several Nb filaments stick out the surface of the wire. One of them is magnified and shown in Figure II-3c. In this figure, part of the filament is in the air , while the rest of it is cold - welded to other filaments. The average diameter of the Nb powders was about 80 microns and the average width of the filaments has become about 5 microns . Since the total volume is not changed , this implies that the average length of the Nb filaments would be 6.8 cm.

(2) Cold - welding between powders was achieved. This effect is reflected in the fact that the wire could be drawn without the supporting cladding after certain reduction and in the micrographs shown in Figure II-3. The welding occurred, presumably, after the surface oxide layers covering the powders had been broken . The same phenomenon was also found in the Nb - Al tape fabricated by rolling thin Nb and Al sheets together[7] and in the powder-metallurgy-processed Cu-Nb-Sn composite wire.[4] The distribution of these broken oxide layers inside the wire and the effect they

Figure II-3. Scanning electron micrographs of three different magnifications showing the configuration of an unreacted Nb 5 wt% Al (80824) wire.

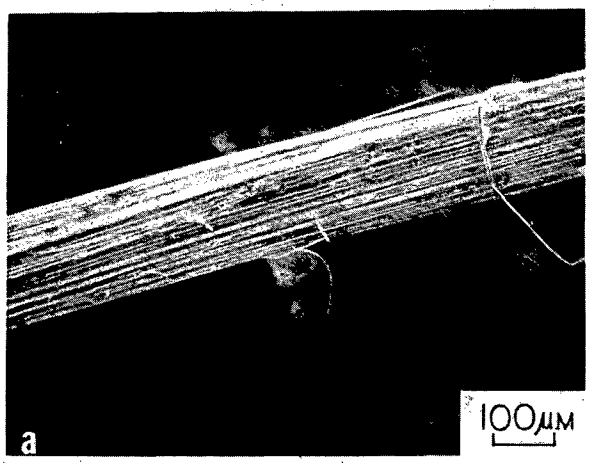

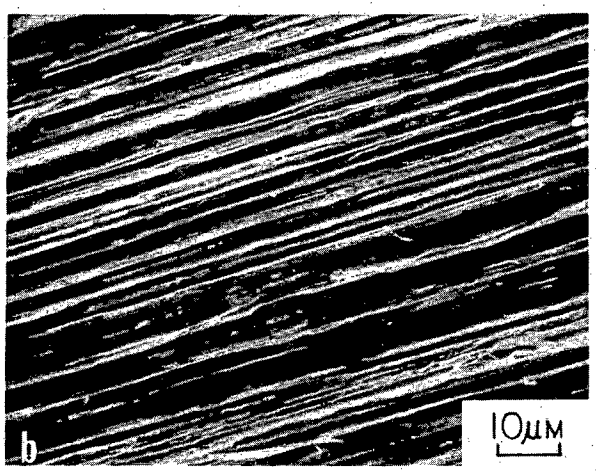

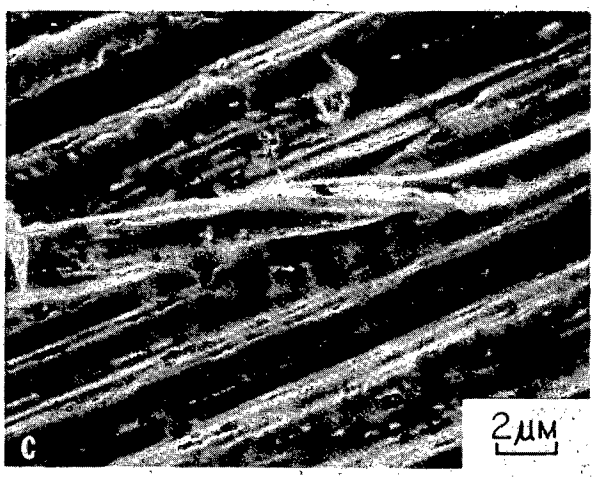

XBB 825-4406

Figure II-3

had on the A15 phase formation mechanism were not clear.

C. Heat Treatments

The deformed powder wires were reacted to form the A15 phase at temperatures ranged from 700 to 1100°C for various periods of time. The cladding material was etched away before heat treatment . The samples were sealed in quartz tubes under an argon atmosphere, and were wrapped with tantalum foils to prevent interaction with the quartz tube. The chemical interaction between the sample and the quartz tube, which could lead to erroneous results, has been reported in other systems.[8] As a further safeguard against contamination, tantalum rods were also sealed into the quartz tube. Single - temperature heat treatments were used to outline the trend of superconducting properties with respect to annealing temperature and time. Based on this trend , multiple - step aging treatments were proposed to optimize the critical temperature (T_c) and overall critical current density (J_c).

D. Superconducting Preperties Measurements

The principal superconducting properties of interest were the critical temperature (T_c) and the critical current density (J_c). The critical temperature was measured by an inductive method using a calibrated germanium resistance thermometer. In principle , the change in magnetic permeability when the sample changes from superconducting to normal state is picked up by a coil around the sample and magnified

through a change in the output voltage . The superiority of the inductive method over the simpler resistance measurement is that it requires no direct electrical contact with the sample. Thus the shape of the sample could be irregular. The resistance measurement usually gives a higher value.

The overall critical current (overall I_c) of the wire was measured using a standard four-probe technique in transverse applied magnetic fields up to 19 teslas. All of the measurements were performed at the National Magnet Laboratory in the Massachusetts Institute of Technology. For comparison and simplicity , I_c was measured at a specific temperature , 4.2 K . After thermal equilibrium had been reached , a uniform magnetic field was applied transversely to the wire direction. The current passing through the wire was then slowly and steadily increased. The critical current at that particular field was defined to be the current at which the potential across voltage leads, spaced 5 mm apart , exceeded 1 microvolt . A typical measurement is shown in Figure II-4 , where the x- and y-axis are the applied current through the sample and the potential difference developed across voltage leads, respectively. The vertical bar in the upper left corner stands for 3 microvolts. The noise is small and the potential difference rises rapidly after the critical current is exceeded. The overall critical current density (overall J_c) was calculated by dividing the overall critical current by the total cross section of the wire, excluding the area of the cladding.

E. Materials Characterization

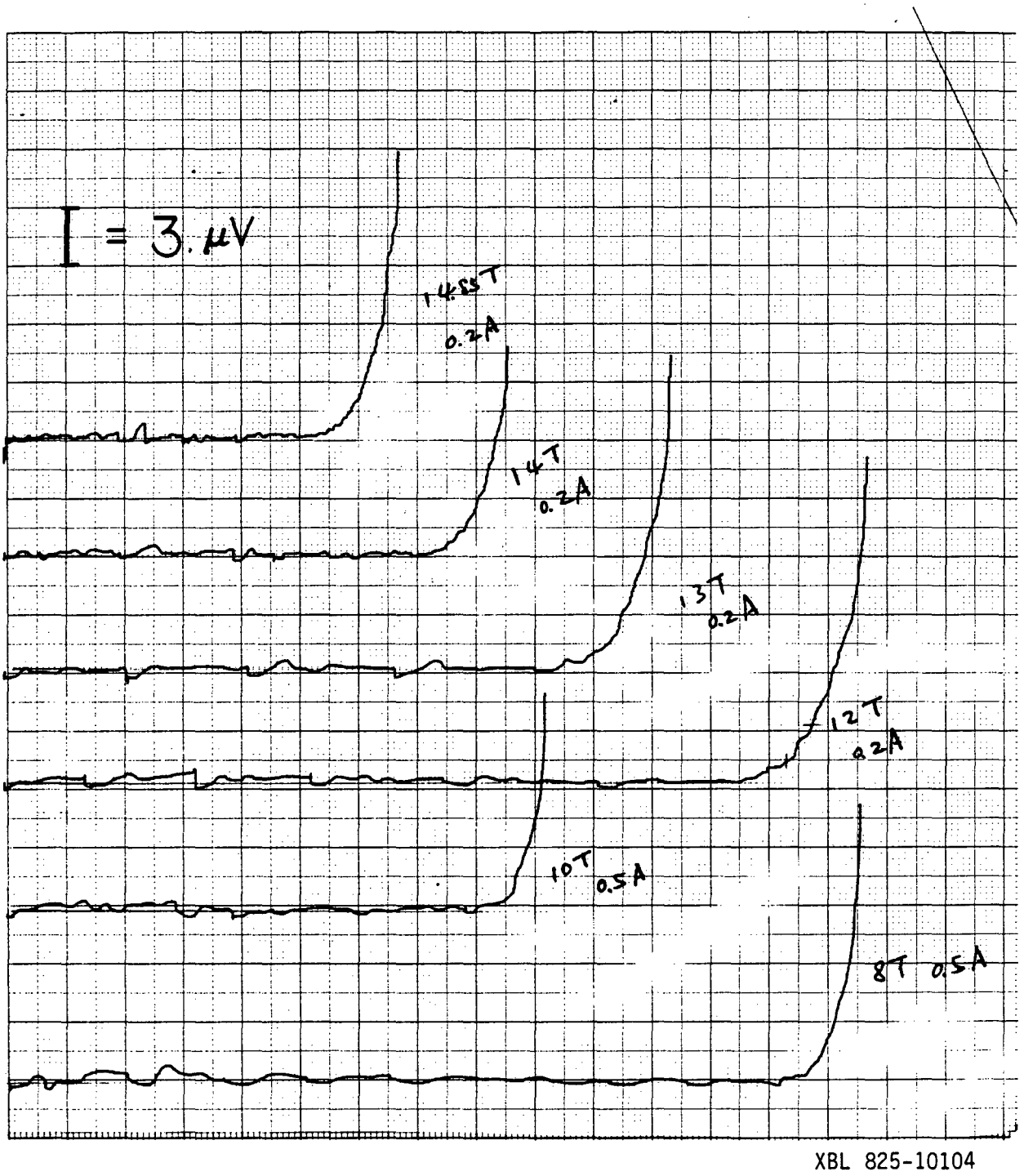
I = 3. μV
14.55T
0.2A
14T
0.2A
13T
0.2A
12T
0.2A
10T
0.5A
8T 0.5A
XBL 825-10104

Figure II-4

The microstructure of the product wire was studied using a combination of conventional x-ray analysis, scanning electron microscopy (SEM), transmission electron microscopy (TEM), and microanalysis . Conventional x-ray analysis was perfomed with both Debye- Scherrer camera and diffractometer and was used for an overall determination of the phases present. Both SEM and TEM were used to observe the microstructural state of the wire and the detailed microstructure of the reacted layer. The microanalysis was performed with a scanning transmission electron microscope equiped with a energy dispersive x-ray spectrometer (STEM/EDS) and was employed to determine the chemical composition of the reacted layer. The SEM study was performed with an AMR 1000 scanning electron microscope operated at 20 kV . The microanalysis and TEM studies were performed with a Philips EM 400 microscope operated at 100 kV.

Samples for x-ray analysis (diffractometer) were made by closely placing several wires together , mounting them in the Koldmount resin , and carefully grinding and polishing by hands using emery papers and diamond paste to obtain a flat surface. Samples for TEM and STEM/EDS studies were made by grinding and polishing the tested wire to a thickness of 0.1 mm or less, followed by gluing the wire to the oval-shaped holder , and ion-milling to obtain sufficient thin areas. In the last step, a Dual Ion Mill 600 manufactured by Gatan Co. was used.

CHAPTER III. RESULTS AND DISCUSSION

To optimize the powder metallurgy (P/M) approach , one needs to characterize at least three parameters of the product wire and to understand the relationships among them. These parameters include the metallurgical characteristics, the superconducting properties, and the processing parameters. The metallurgical characteristics include the phases present in the reacted layer, their microstructures and morphologies, in particular, the grain size, chemical composition and distribution of the superconducting A15 Nb_3Al phase. The principal superconducting properties of interest are the critical temperature (T_c) and the overall critical current density (overall J_c). The processing parameters , described at length in the last chapter , include the powder size, the powder size ratio between Nb and Al, the areal reduction ratio (R), and the heat treatment.

In general, the processing parameters would determine the metallurgical characteristics of the product wire, and the superconducting properties would be influenced by the metallurgical characteristics.

A. Metallurgical Characteristics

A.1. Preferred Orientation and Configuration of the Unreacted Wire

The deformed powder wire exhibited a [110] preferred orientation along the wire axis due to the aligned Nb filaments. Figure III-1 is a powder photograph of an unreacted sample of 5 wt% Al (80824) taken with a Debye - Scherrer camera. The texture is clearly revealed near

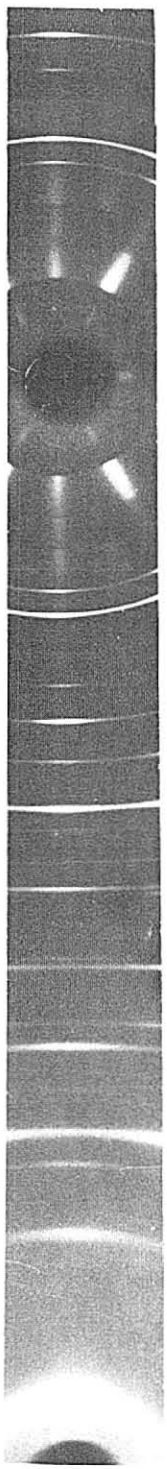

XBB 825-4404

Figure III-1

the $2\theta = 0$ end on the right of the figure. The pattern is similar to the ideal [110] texture[1] shown in Figure III-2. The arcs, symmetrically centered about the ideal spot positions, have replaced the spots. The intensity of the arcs is the largest at their centers, indicating that more planes in Nb filaments tend to have the ideal inclination with the wire axis. There are less and less planes deviating from the ideal value as the deviation increases. The texture still existed even after the wire had been reacted at 900°C for 25 hours. The preferred orientation of the Al filament along the wire direction is believed to be [111], the close - packed direction of face - centered cubic structures. Limited by the equipment available, the more favorable transmission Laue method in studying the texture was not performed. The deformation of the Nb powder itself is also reflected in the very high dislocation density in the residual Nb filament, which is evident from the TEM study.

The SEM and optical analyses of the unreacted powder wire suggest that the deformed wire contains a continuous filamentary matrix of Al in the interstices of the Nb powders. The transverse and longitudinal cross sections of two unreacted Nb 5 wt% Al wires are shown in the scanning electron micrographs in Figure III-3. "T" and "L" stand for transverse and longitudinal cross sections, respectively. The Al has been etched away to reveal the surrounding Nb matrix.[2] The sample of lower reduction is shown in Figure III-3a and 3b. Nb powders are slightly elongated along the wire direction and are still irregularly-shaped at such a low reduction. For samples of much higher reductions, as illustrated in Figure III-3c and 3d, Nb powders were deformed into parallel filaments of nearly uniform thickness. The magnification here

Figure III-2. Patterns of ideal [111] and [110] wire textures.

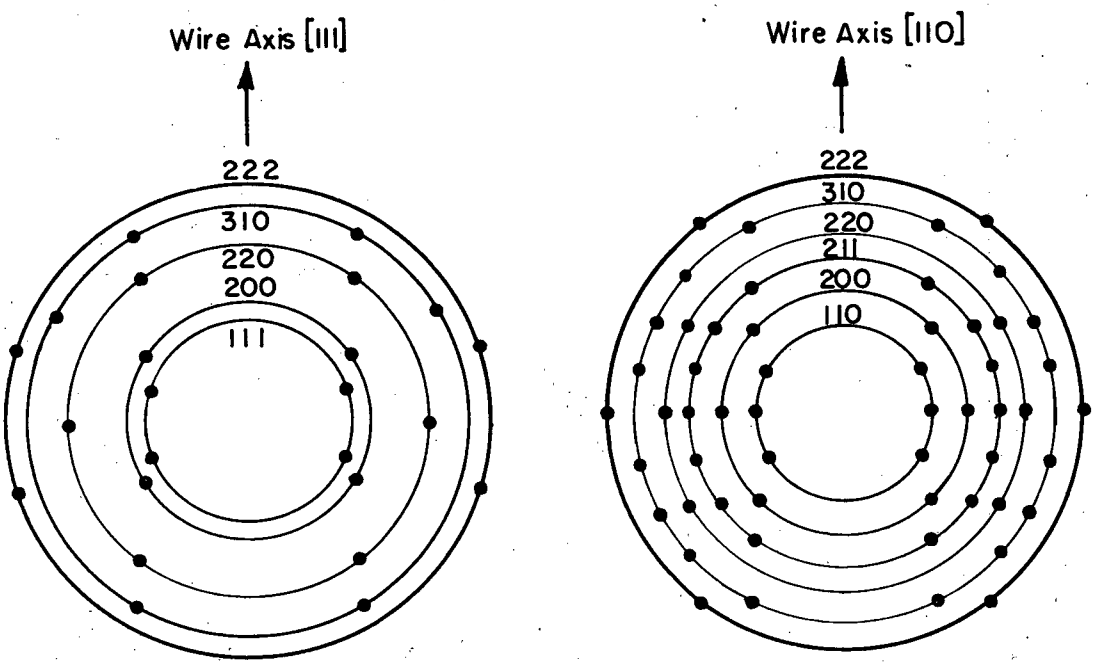
Wire Axis [111]
222
310
220
200
111
Wire Axis [110]
222
310
220
211
200
110
XBL825-5679

Figure III-2

Figure III-3. Scanning electron micrographs of the transverse (T) and longitudinal cross sections (L) of unreacted Nb 5 wt% Al (811027) samples with two different areal reduction ratos (R = 40 and 7640).

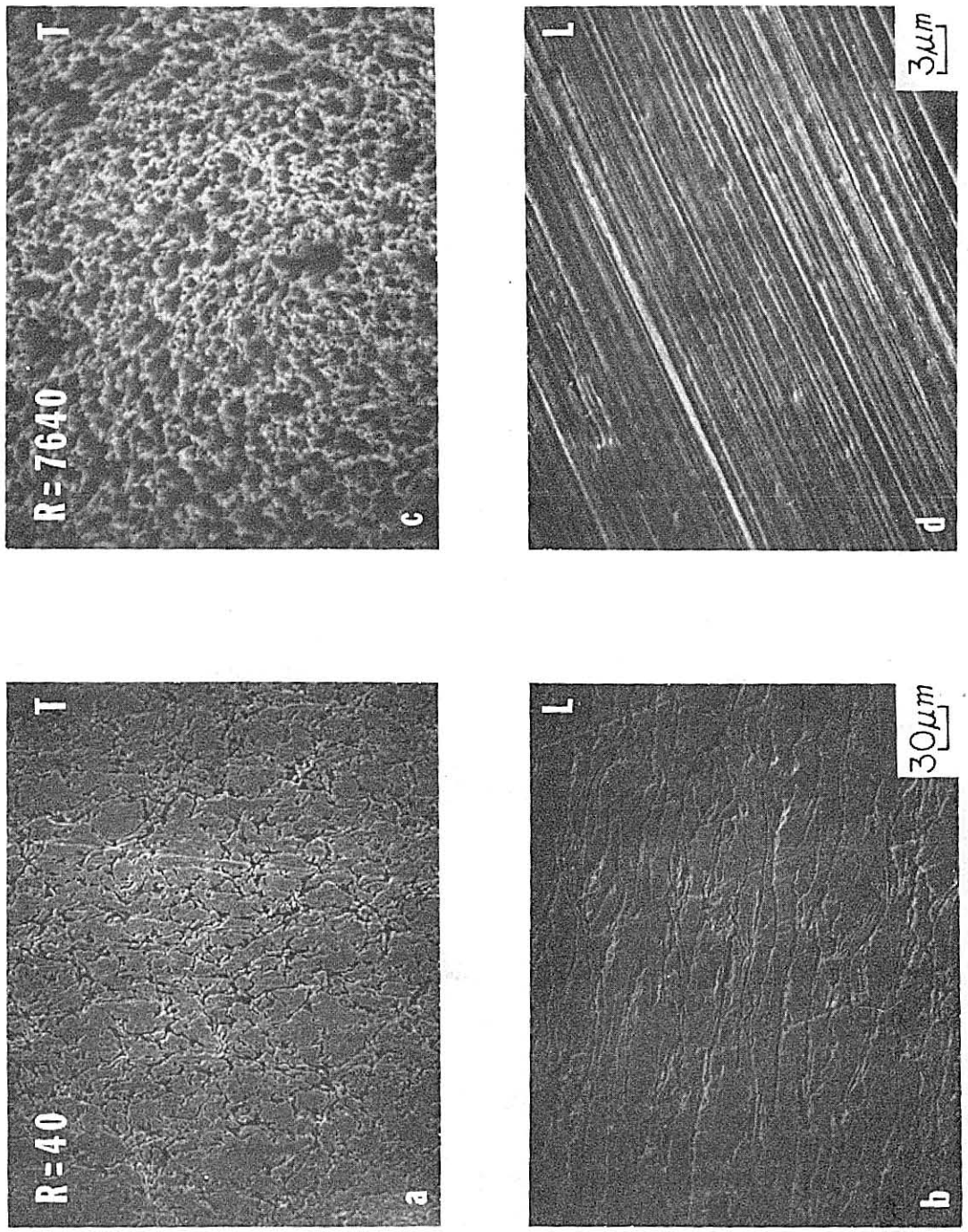

XBB 825-4820

Figure III-3

has been increased by an order of magnitude to more closely examine the configuration of the wire. It is noticed that Al filaments have irregular shapes and are more like ribbons. Nb filaments seem to have formed a continuous matrix and are indistinguishable from one another. This confirms that the Nb powders have been cold - welded together by the deformation processs , as described in the last chapter. It is perceived that the reacted layer would also be ribbon - like. This is indeed the case, as will be shown later for samples of 5 wt% Al heat-treated at 900°C for 22.5 minutes.

A.2. The Phases Present

The reaction to form the A15 superconducting phase occurs at the interface between the Nb and Al. Since the reaction temperature is in all cases above 660°C, the melting point of the pure Al, the initial reaction is between liquid and solid phases . Reference to the binary Nb - Al phase diagram (Figure III-4) shows that three intermetallic compounds can be formed between Nb and Al at temperatures ranged from 700 to 1100°C.[3] These compounds are the A15 phase, Nb_3Al, the σ-phase, Nb_2Al , and the aluminum-rich intermetallic , $NbAl_3$. All these phases are expected to form along the solid-liquid interface.

The phase distribution in the reacted samples was studied by x-ray analysis and by conventional TEM in conjunction with STEM/EDS. The x-ray analysis , using the Debye - Scherrer method , of samples of 5 wt% Al (80824) reacted at 750 - 1100°C for various periods of time revealed only Nb and σ- phase reflections. This result suggests that the A15 phase is not the major constituent , but does not necessarily

Figure III-4. Equilibrium binary Nb-Al phase diagram (Lundin and Yamamoto, 1966).

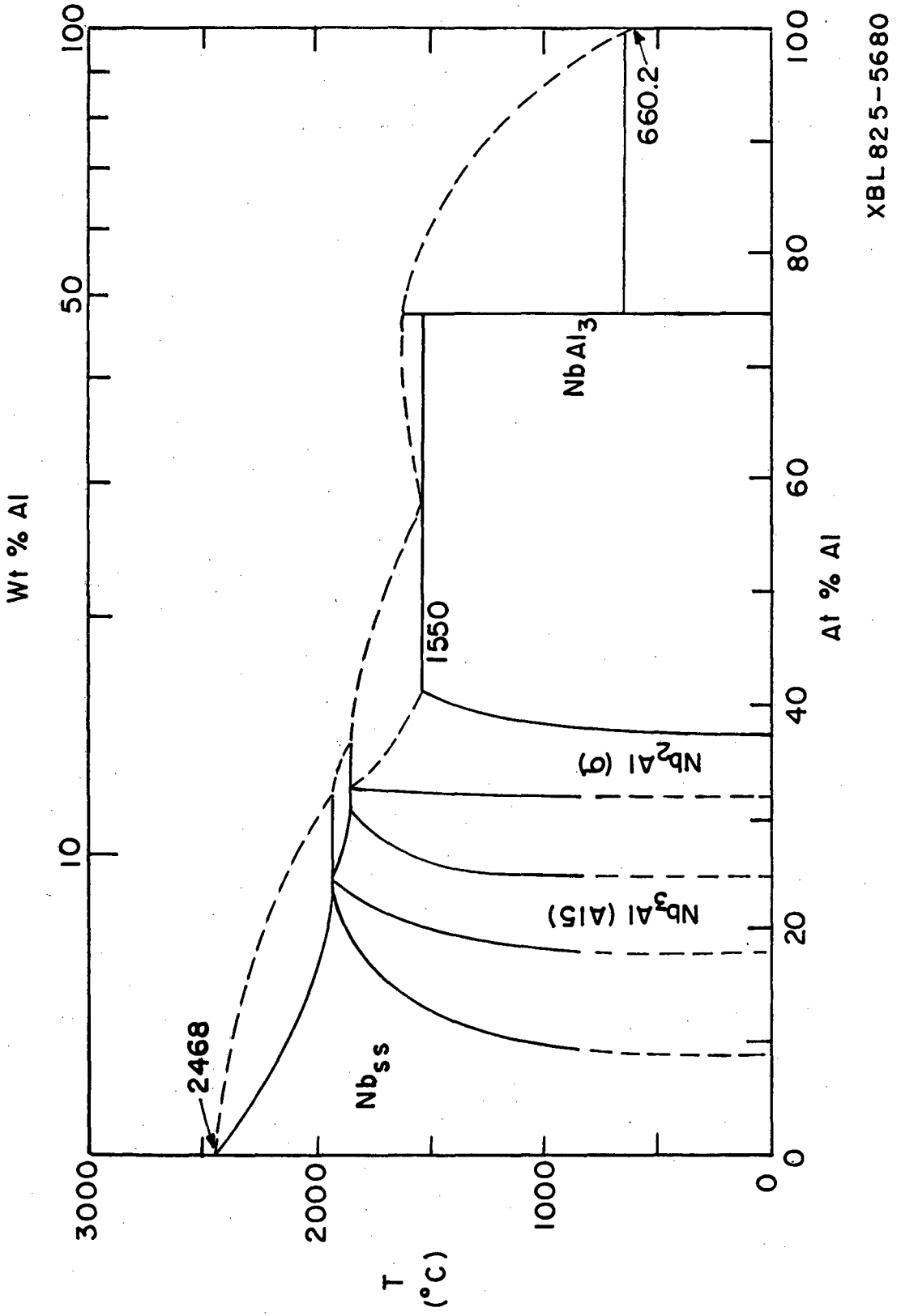
Wt % Al
At % Al
T (°C)
3000
2000
1000
0
100
50
10
0
20
40
60
80
100
660.2
NbAl3
1550
Nb2Al (σ)
Nb3Al (A15)
Nbss
2468
XBL825-5680

Figure III-4

show an inadequate content of the A15 phase because of the complexity of its diffraction pattern and the consequently low intensity of its diffraction peaks. The presence of the A15 phase in these samples is revealed by TEM and STEM/EDS studies and by the fact that the product wire can have a T_c onset of 15.5 K in the absence of the applied magnetic field and an overall J_c of approximately 5×10^3 A/cm^2 in a transverse applied magnetic field of 12 teslas at 4.2 K . The A15 diffractions peaks were later identified in samples of better overall J_c values with a diffractometer (see Figure III-25) . The $NbAl_3$ phase was also observed in several samples with a transmission electron microscope.

A.3. Microstructure and Morphology

As mentioned in the last section , x-ray studies were unable to detect the presence of Nb_3Al and $NbAl_3$ phases in reacted 80824 samples. It was therefore necessary to look into the local morphology of the reacted interface using a high-resolution transmission electron microscope.

A TEM micrograph of the longitudinal cross section of a 80824 sample reacted at 1100°C for 1 minute is shown in Figure III-5. Three distinct morphologies are present at the previous Nb - Al interface. The residual Nb phase , lying in the lower left corner , is characterized by a fine microstructure and a high dislocation density. The dislocations are remnants of the wire drawing process and are not recovered after 1 minute at 1100°C , which is only about one half of the Nb melting point in the absolute temperature scale. Adjacent to

Figure III-5. Transmission electron micrograph of a 5 wt% Al (80824) sample annealed at 1100°C for 1 minute.

XBB 813-2376

Figure III-5

the Nb interface, there is a fine - grained region, which microanalysis shows to be a mixture of the A15 and σ - phases. Beyond the fine-grained region is a coarser- grained layer of $NbAl_3$. No residual Al was found.

Three typical x-ray energy spectra for the A15 , σ- , and $NbAl_3$ phases are shown in Figure III-6. They were acquired by the STEM/EDS using a convergent electron-beam of a diameter of 100 Å . The total counts of the whole spectrum was preset to 100,000 as a standard. The x- and y-axis are the energy in kev and the intensity in counts , respectively. In the middle spectrum, which was due to the σ -phase, the scale of y-axis was deliberately doubled to show the low- intensity background. In the spectra for the A15 and $NbAl_3$ phases the background had been substracted first and , after the resultant spectra were plotted, was superimposed and plotted as a seperate curve for comparison. As shown in the figure the Al K_α , Nb L_α , Nb K_α , and Nb K_β peaks are well seperated and can be indentified without any difficulty. It is clear that the peak-height ratio between the Al K_α and any of the Nb peaks, e.g., Nb L_α , increases from the Nb_3Al to Nb_2Al and $NbAl_3$ spectra (from the top to the bottom in the figure).

Because of the complex microstructure of the material present in the A15- σ-phase mixture and the limited image resolution of the detector employed , it was not possible to separate the two phases by the STEM/EDS used in this study. However, if the sample was given a longer annealing at 1100°C, the A15 and σ-phases separate into distinct layers and the $NbAl_3$ phase is consumed. The micrographs in Figure III-7 illurstrate the microstructure after 1.5 hours annealing at 1100°C. Figure III-7a shows the A15 grains , which now have an average grain

Figure III-6. Three typical x-ray energy spectra of Nb_3Al (A15), Nb_2Al (σ), and $NbAl_3$ phases acquired by a STEM/EDS.

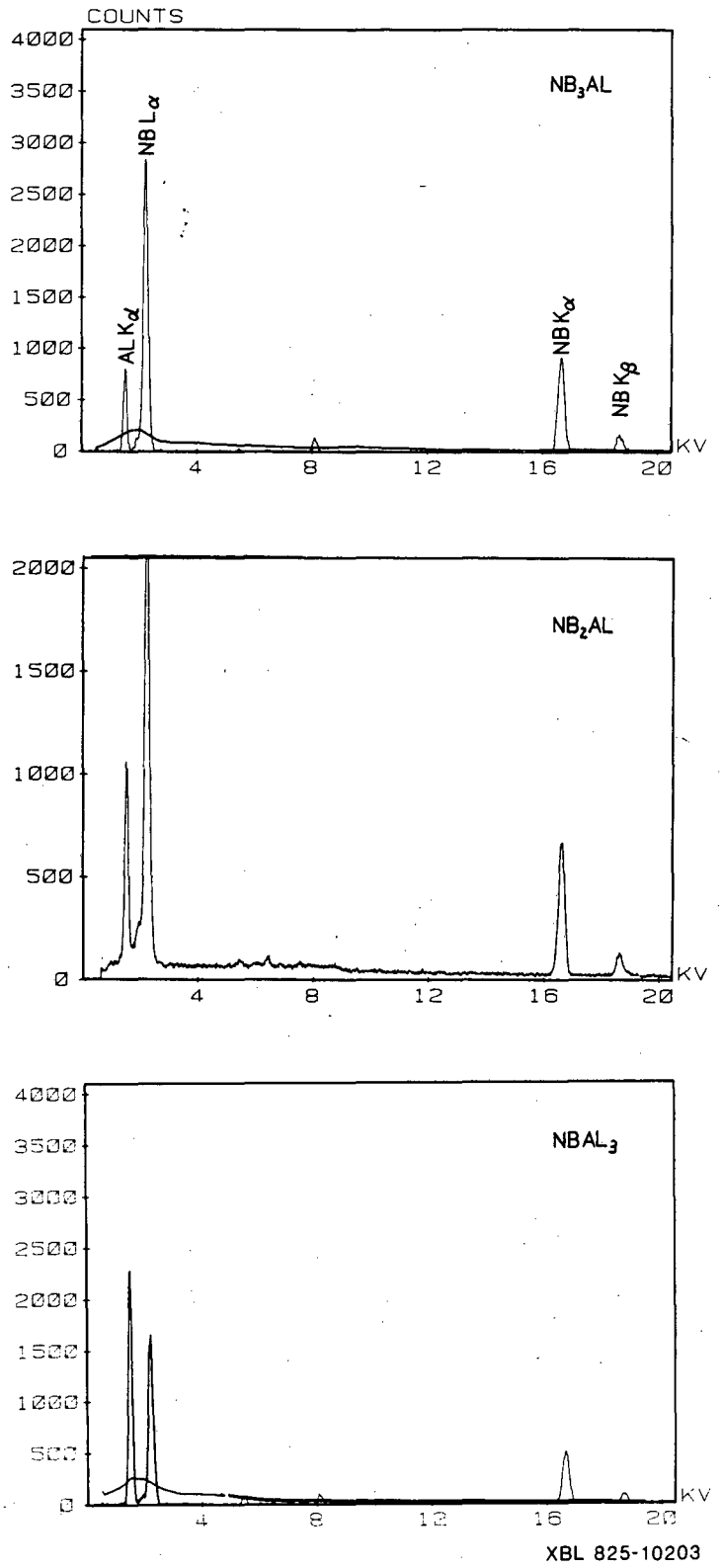
COUNTS
4000
3500
3000
2500
2000
1500
1000
500
0
NB$_3$AL
NB Lα
AL Kα
NB Kα
NB Kβ
KV
4
8
12
16
20
2000
1500
1000
500
0
NB$_2$AL
KV
4
8
12
16
20
4000
3500
3000
2500
2000
1500
1000
500
0
NBAL$_3$
KV
4
8
12
16
20
XBL 825-10203

Figure III-6

Figure III-7. Transmission electron micrographs of a 5 wt% Al (80824) sample annealed at 1100°C for 1.5 hours: (a) A15 region and (b) σ-phase.

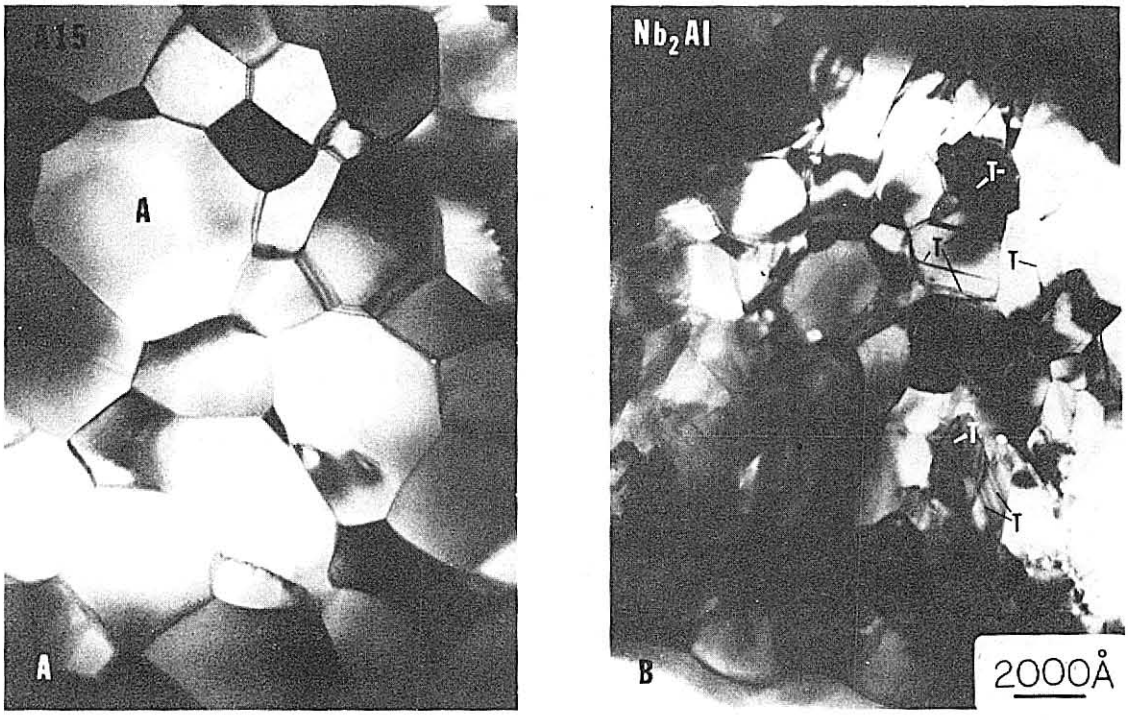

XBB 826-4977

Figure III-7

size of about 3000 Å. They are equi- axed and almost free of lattice defects. Obviously the grain growth has already started; for example, the grain with 10 sides , denoted by "A", appears to be consuming the smaller surrounding grains . The σ grains , on the other hand , are internally defective, as shown in Figure III-7b. The dark bands within these grains, e.g., those denoted by "T's", are revealed to be crystallographic twins by the microstrutural analysis. A high - magnification TEM image of the twins in the same sample is shown in Figure III - 8. The width of the twins is typically of ~ 350 Å .

It appears likely that the difference in defect characteristics can be used to distinguish the A15 and σ-phases in the fine-grained layer which results from the initial reaction. A re-examination of Figure III-5 shows that the grains in the fine - grained region are a mixture of defect - free and twinned grains. It is tentatively assumed that the twinned grains represent the σ- phase, while the defect- free grains represent the superconducting A15 phase. The grains , having parallel black and white contrast and being on the top of the A15-σ mixture, are believed to be thin layers of Nb. These Nb layers were parts of the residual Nb filament that was originally on the top of the reacted region. They were not completely etched away by the ion-thinning process. This conclusion is supported by the TEM micrograph shown in Figure III-9, which shows the reacted layer between two residual Nb interfaces of a sample of 3 wt% Al (810422) annealed at 800°C for 16 hours. The Nb filament on the left is almost etched away. It has very similar contrast , e.g., those denoted by "N's", to that of the thin Nb layers in Figure III-5. It is noticed that the width of the reacted layer in this micrograph is about 0.9 microns , which is

Figure III-8. Transmission electron micrograph of the σ-phase of a Nb 5 wt% Al (80824) sample annealed at 1100°C for 1.5 hours showing the crystallographic twins.

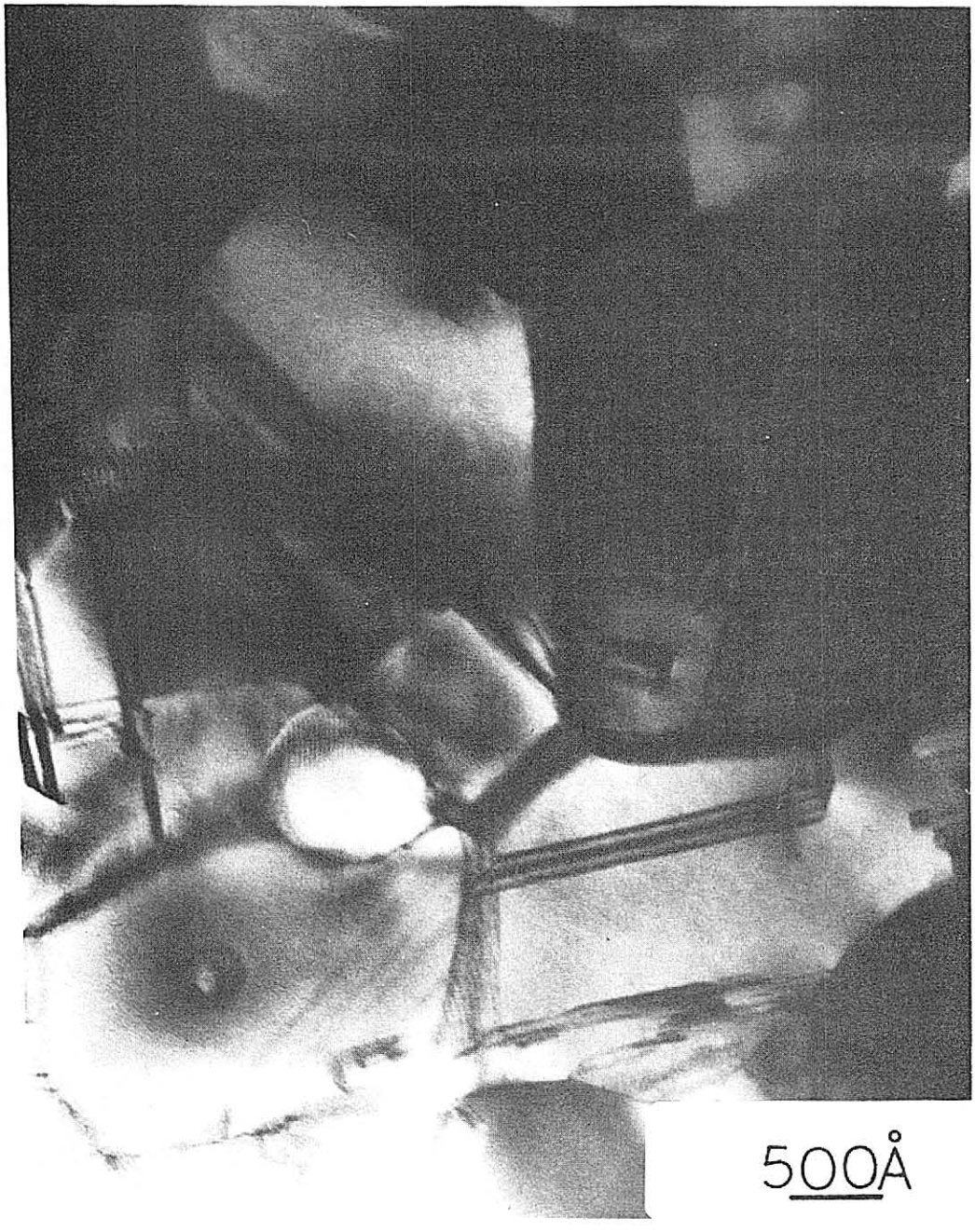

XBB 824-4037

Figure III-8

Figure III-9. Transmission electron micrograph of a 3 wt% Al (810422) sample annealed at 800°C for 16 hours showing the microstructure of the reacted layer between two residual Nb regions.

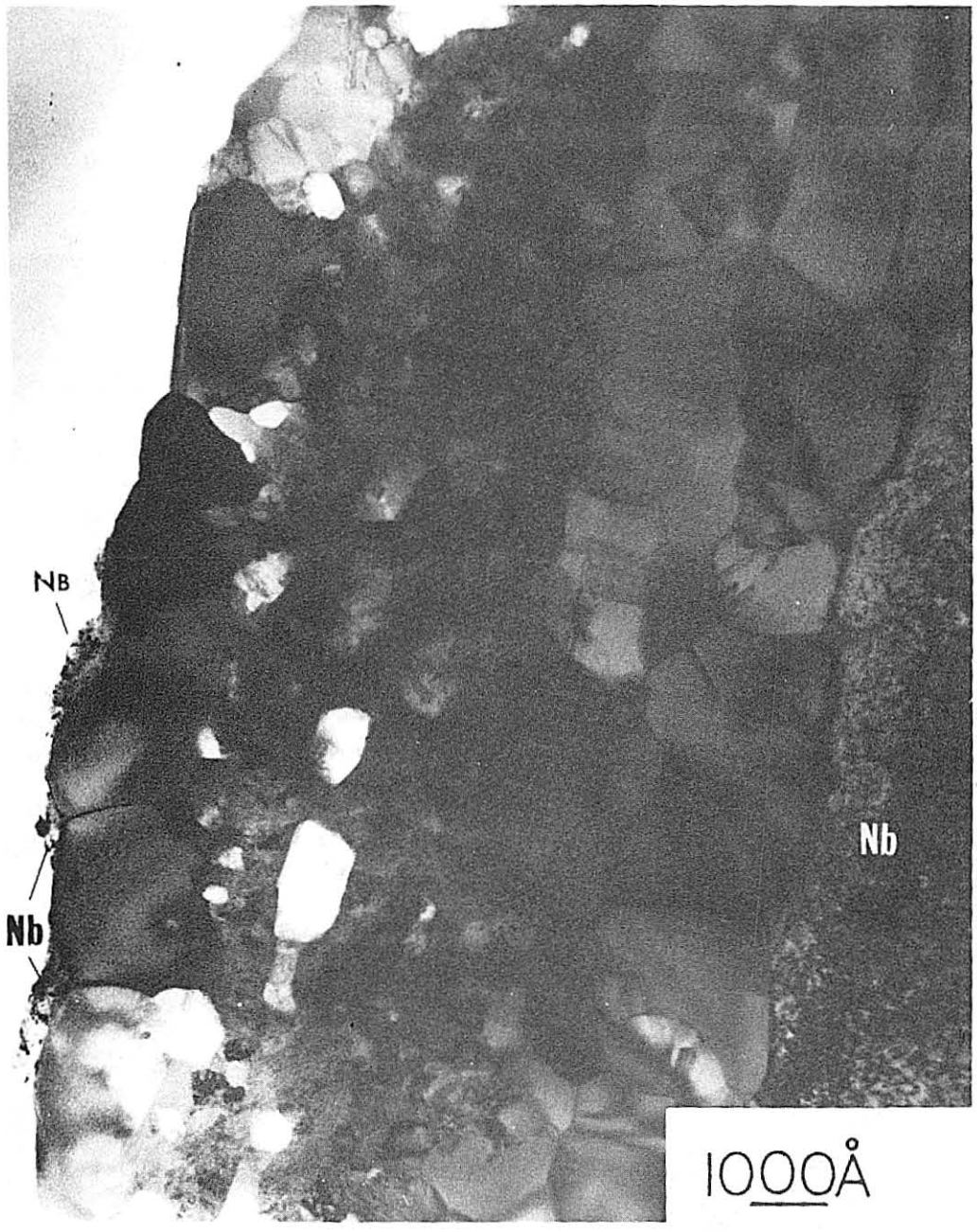

XBB 824-4036

Figure III-9

smaller than that usually observed in the "Bronze"-processed sample.

Figures III-10 and 11 show other areas of the same sample shown in Figure III-9. This sample was taken from a superconducting wire which exhibited an overall J_c above 10^4 A/cm^2 in a magnetic field of 13 T at 4.2 K . The microstructure adjacent to the Nb interface, again , contains a mixture of A15 and σ-phases. The $NbAl_3$ phase was not observed. If it is assumed that the substructurally twinned grains constitute the σ-phase, then it appears that the σ -phase has a higher volume fraction within the fine-grained layer. However, locally there is a sufficient volume of the defect-free A15 phase to establish a reasonably interconnected , fine - grained structure . Both the fine grain size and the interconnectivity of the A15 grains are reflected in the high critical current of the sample. It is noticed , furthermore, that the width of the reacted layer varies from larger than one micron down to as small as 950 Å in Figures III-9, 10, and 11. This non-uniformity results from the rather large range of the powder sizes employed (see Table II-1).

B. Control and Optimization of T_c and Overall J_c by Heat Treatments

The P/M approach can be separated into three consecutive processes, namely, the powder preparation, the mechanical deformation, and heat treatments. These processing parameters can influence the resultant metallurgical characteristics , which in turn determine the superconducting properties of the product wire. Ideally, the relationships among the processing parameters , the metallurgical characteristics, and the superconducting properties should be examined separately.

Figure III-10. Transmission electron micrograph of a 3 wt% Al (810422) sample annealed at 800°C for 16 hours.

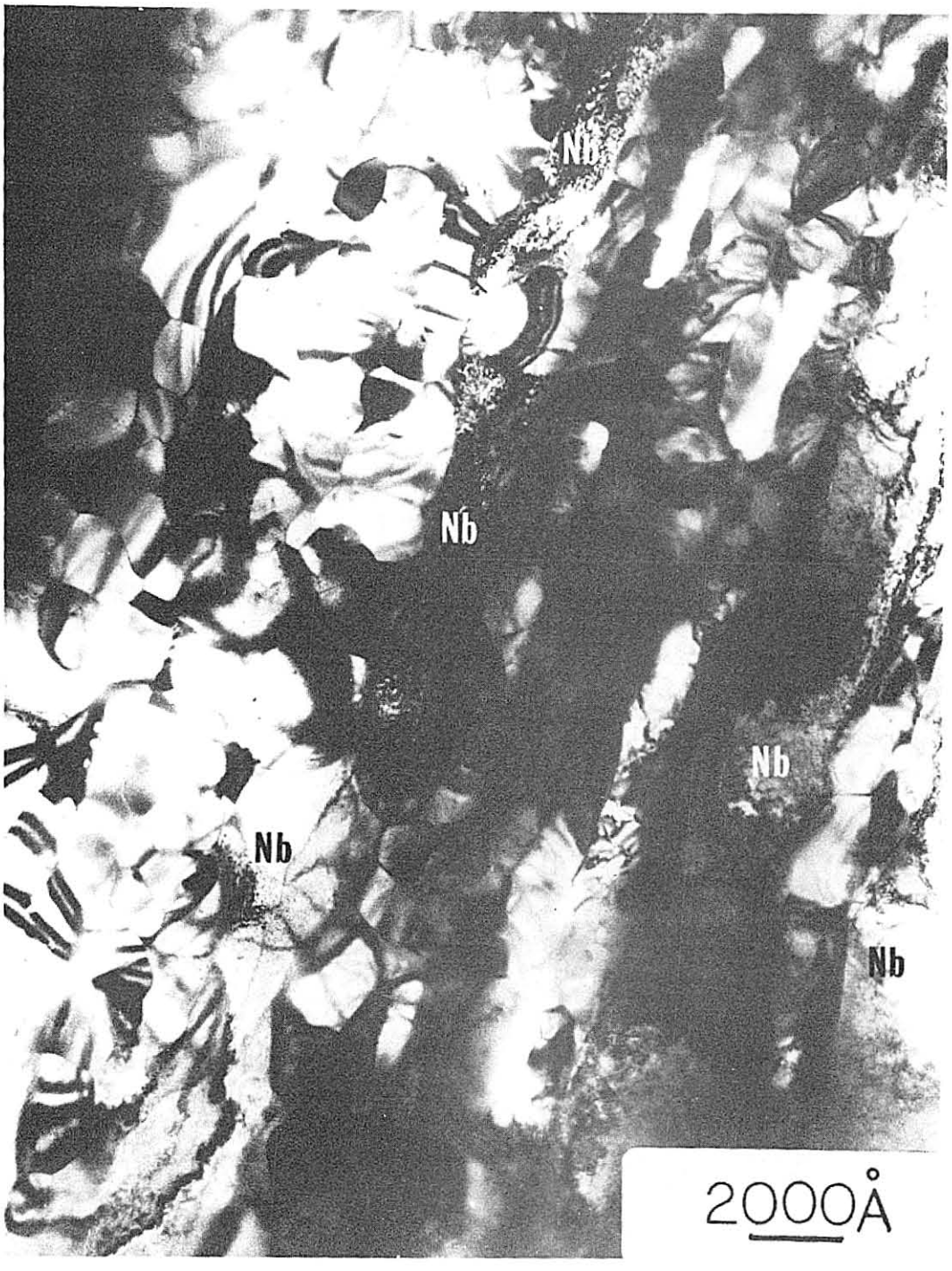

XBB 815-4615

Figure III-10

Figure III-11. Transmission electron micrograph of a 3 wt% Al (810422) sample annealed at 800°C for 16 hours.

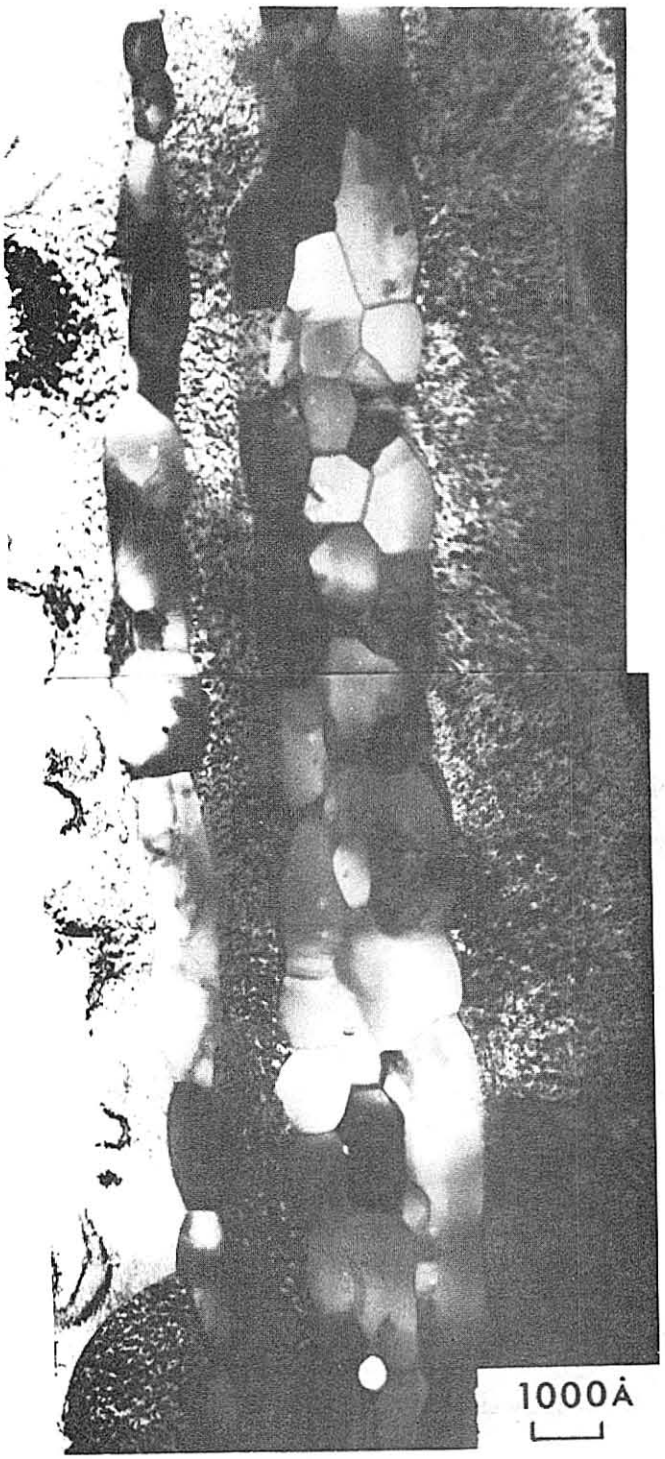

XBB 824-4031A

Figure III-11

Practically , however , one would first vary the processing parameters and measure the superconducting properties, then look into the metallurgical characteristics to try to correlate them. In the following few sections , the variations of T_c and overall J_c with each processing parameter will be presented and discussed.

B.1. T_c and Single-Temperature Heat Treatments

The critical temperature of the P/M processed Nb_3Al phase was measured as a function of annealing time and temperature. The results for the 5 wt% Al (80824) samples, given single-temperature heat treatments, are plotted in Figure III-12. Irrespective of the temperature range employed (700 - 1100°C), the critical temperature rises slightly on initial annealing and reaches a maximum at approximately 15.5 K. It then tends to decrease with longer annealing time. The kinetics of this characteristic behavior depends strongly on the temperature of the heat treatment used. The superconducting-to-normal transition width is less than 1 K in most cases. Similar behaviors are also observed in other samples. The high-peak critical temperature exhibited by these specimens is surprising since the A15 phase in equilibrium with the σ -phase at temperatures of 1100°C or below is expected to have a maximum critical temperature of only about 14.4 K . This value was estimated in the following way: Shown in Figure III-13 is the equilibrium binary Nb-Al phase diagram in the vicinity of the stoichiometric composition of the A15 phase , which was reported by Jorda et al.[4] According to this diagram , the boundary between the single-phase (A15) region and the two-phase (A15 + σ) region at 1100°C is at ~ 21.7

Figure III-12. Critical temperatures of 5 wt% Al (80824) samples as a function of annealing temperature and time.

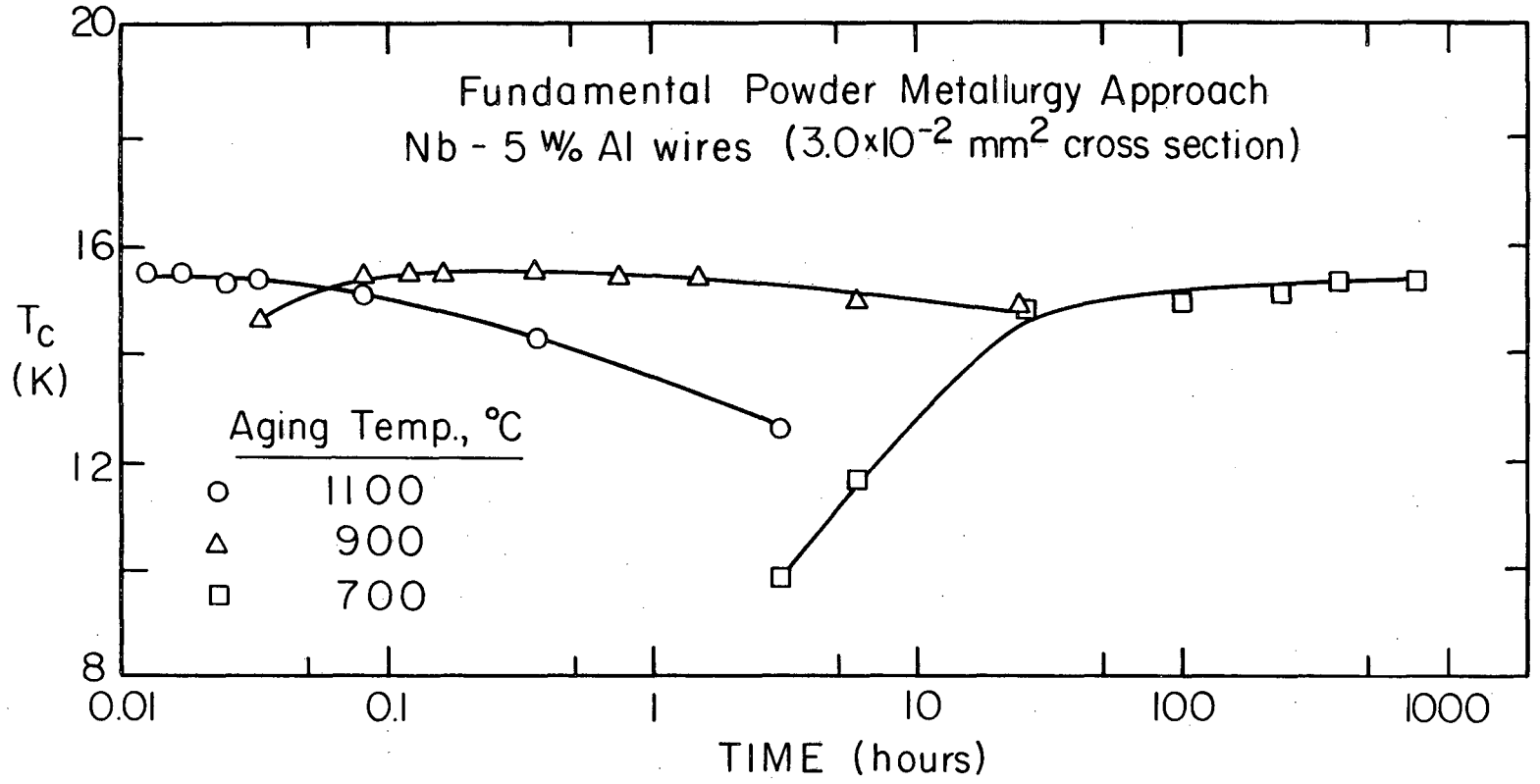

Figure III-12

Figure III-13. Equilibrium binary Nb-Al phase diagram in the vicinity of the stoichiometric composion of the A15 phase (Jorda et al., 1981).

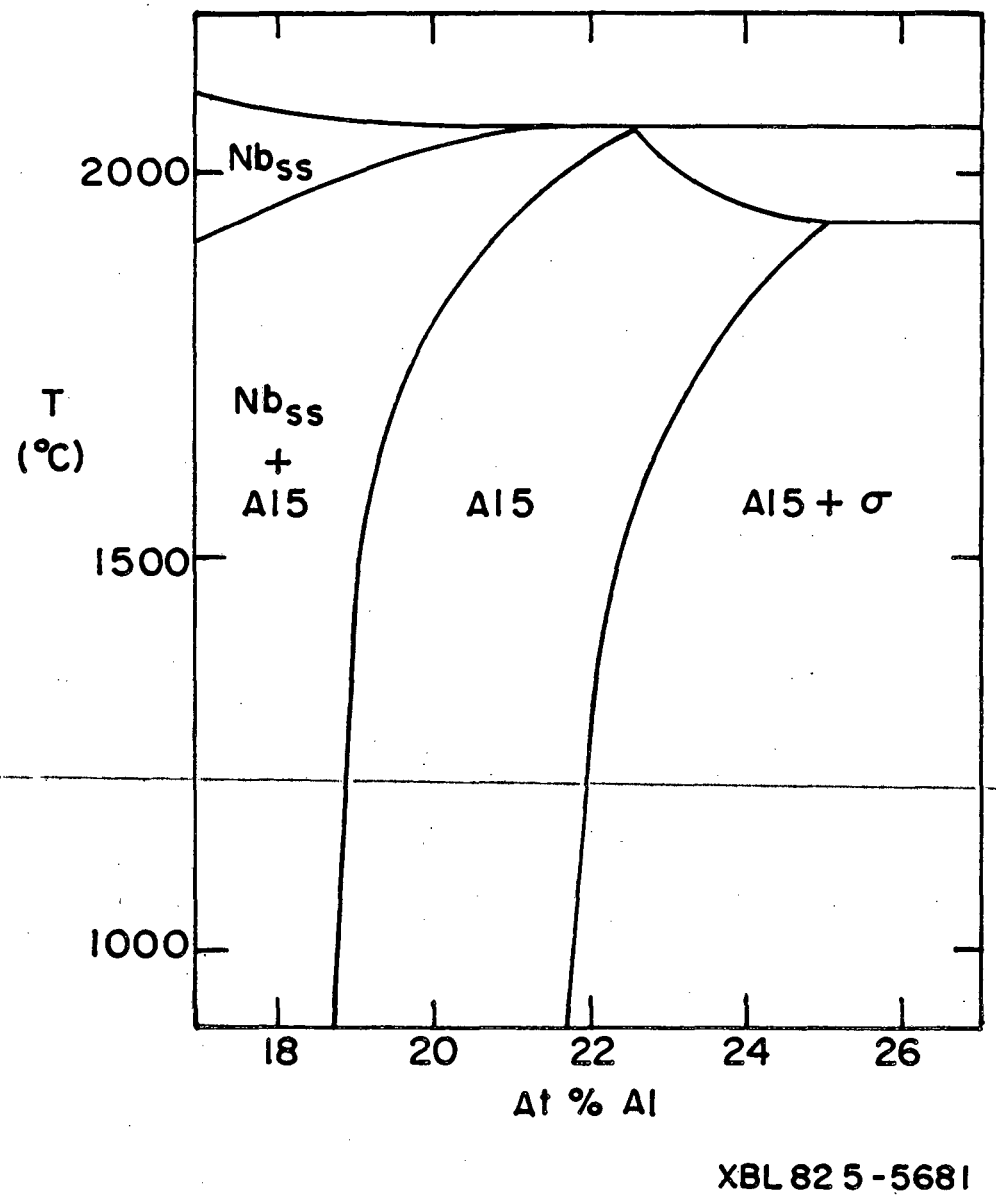

Figure III-13

at% Al. Kwo et al.[5] found that the increment of T_c with Al composition, i.e., $\Delta T_c/\Delta C$, was 1.9 K/at% Al. The maximum T_c of the A15 phase they predicted was 20.7 K at the stoichiometric composition. Therefore , one can derive the T_c at 21.7 at% Al to be 14.4 K . Here it has been assumed that the T_c is a function only of the composition in the A15 phase even in the presence of the σ-phase.

The reason for the high T_c is not yet clear, but may be due to the following factors: (1) the heat of formation resulted from the initial chemical reaction , and/or (2) the release of the elastic energy stored during the very heavy cold-working . These two energies could locally raise the temperature higher than that of the furnace . It is also possible that the reaction in the product wire , which forms A15 grains of submicron sizes , cannot be simply explained by the result derived from the bulk or relatively homogeneous samples.

B.2. T_c and Multiple-step Heat Treatments

It is generally accepted that the critical temperature of the A15 phase is determined by both its chemical composion and its long range order.[6] From the equilibrium phase diagram (Figures III-4 and 13), high temperature treatments tend to promote a more nearly stoichiometric composition of the A15 phase. Heat treatments at lower temperatures , on the other hand , are expected to establish a better state of long range order. In an attempt to improve the inherent characteristics of the A15 phase, multiple-step treatments were therefore proposed, beginned with a high temperature treatment to establish a optimum composition followed by an annealing at lower temperatures

with the intent of improving the internal state of order. These double - step treatments appear to be successful in substantially improving the T_c onset. For example, a treatment of a 5 wt% Al sample at 1100°C for one minute followed by 900°C for 22.5 minutes increased the T_c onset from 15.5 to 16.3 K . The result is plotted in Figure III-14. The open circles represent the variation of the critical temperature with time for samples annealed at 1100°C. The improvement of the T_c onset by the double-step treatment of 1100°C/1 minute plus 900°C for various periods of time is represented by open triangles . The critical temperature rises on the initial annealing , reaches a maximum at 16.3 K, and then tends to decrease on further annealing. This behavior is similar to that of the single temperature treatment. Therefore , a third- step annealing at 750°C was added to the optimal double- step treatment to try to further increase the critical temperature . The result is also plotted in Figure III-14 and is represented by open squares , which illustrates that the T_c onset is subsequently increased to 17 K by a combination of 1100°C/1 minute plus 900°C/22.5 minutes plus 750°C/8 days. Further annealing was not performed, though the T_c onset seems to be still increasing. It is , of course , possible that these measured critical temperatures reflect the properties of the best of the superconducting material , and are not typical of the average material within the superconducting layer. On the other hand , the superconducting-to-normal transition width, represented by the vertical bar , remains to be small and is ~ 1 K , which suggests that a general improvement of the A15 material has been obtained.

It is interesting to note that the maximum T_c onsets of samples of number 80824, 810422, and 811027 given single-temperature treatments

Figure III-14. Critical temperatures of 5 wt% Al samples as a function of annealing temperature and time.

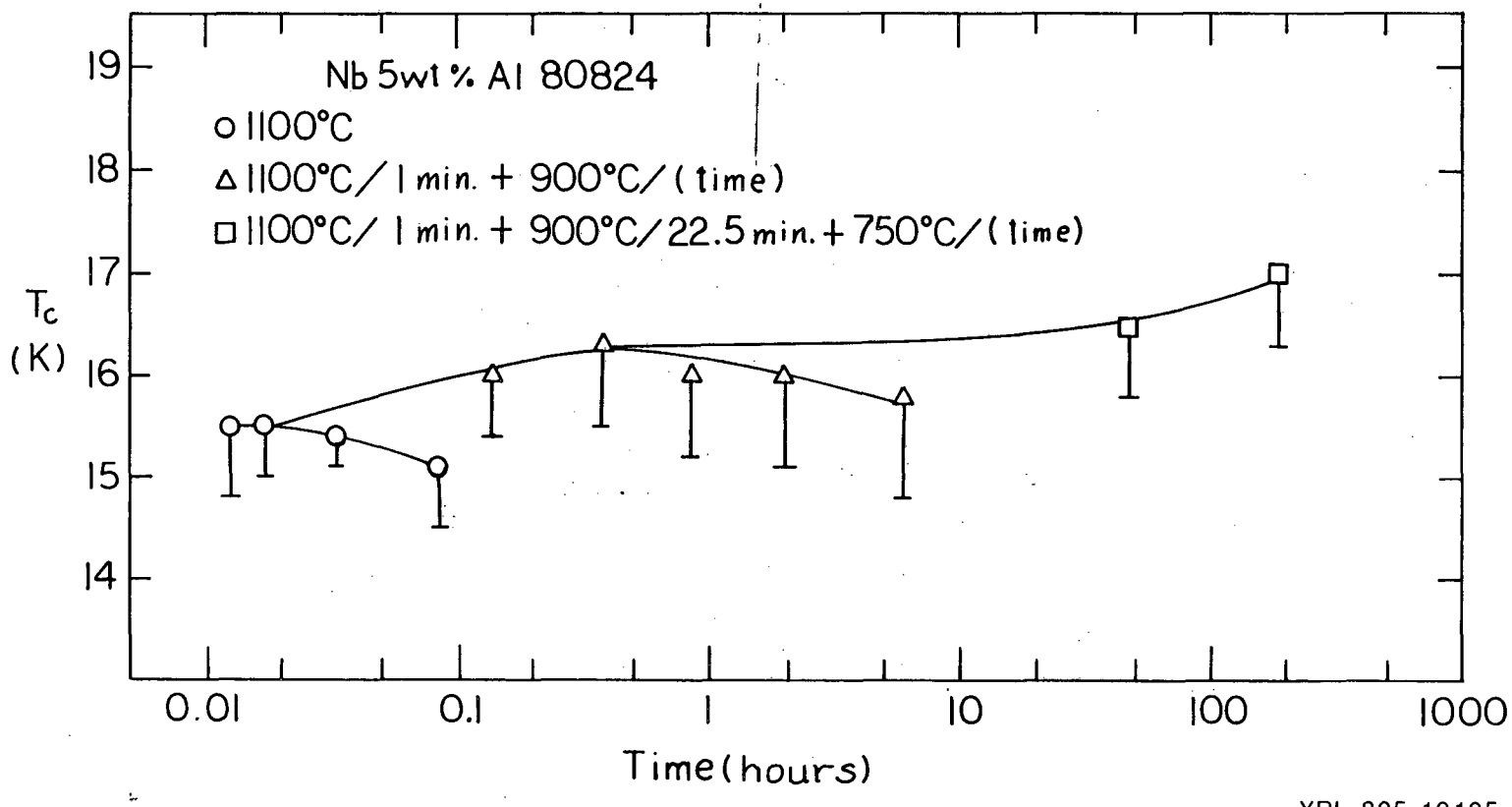

XBL 825-10105

Figure III-14

at 900°C are in the increasing order of 15.5, 16.0, and 16.2 K, respectively. The areal reduction ratio of these samples also increases in that order. However , no conclusion can be drawn for the moment since other parameters , e.g., powder size and Al content , also vary from sample to sample.

Other samples also showed improvements of T_c when given double-step treatments. The T_c onset of a sample of 3 wt% Al was raised from 16 to 16.6 K , an increase of 0.6 K , when first heated at 900°C for 22.5 minutes and followed by an annealing at 750°C for 4 days, as shown in Figure III-15 . If the temperature used in the first step of the double-step treatment were higher than 900°C, but with the same second-step treatment , a higher T_c would possibly be obtained since at the first treatment a better chemical compostion of the A15 phase would be established. A combination of 1100 and 750°C was performed and the result is plotted in Figure III-16. The T_c onset was increased from 15.7 to 16.8 K, an increase of more than 1 K, when a sample was treated at 1100°C for 1 minute and followed by an annealing at 750°C for 4 days.

B.3. Overall J_c and Heat Treatments

The current- carrying capacity of an A15 superconducting wire depends strongly on the volume fraction , chemical composition , grain size, and continuity of the A15 phase in the product wire. If the A15 phase is not the major constituent in the reaction layer and is not continuous , other factors , such as proximity effect , must be taken into account. As described in sections A.1-3 , the microstructure in

Figure III-15. Critical temperatures of 3 wt% Al (810422) samples as a function of annealing temperature and time.

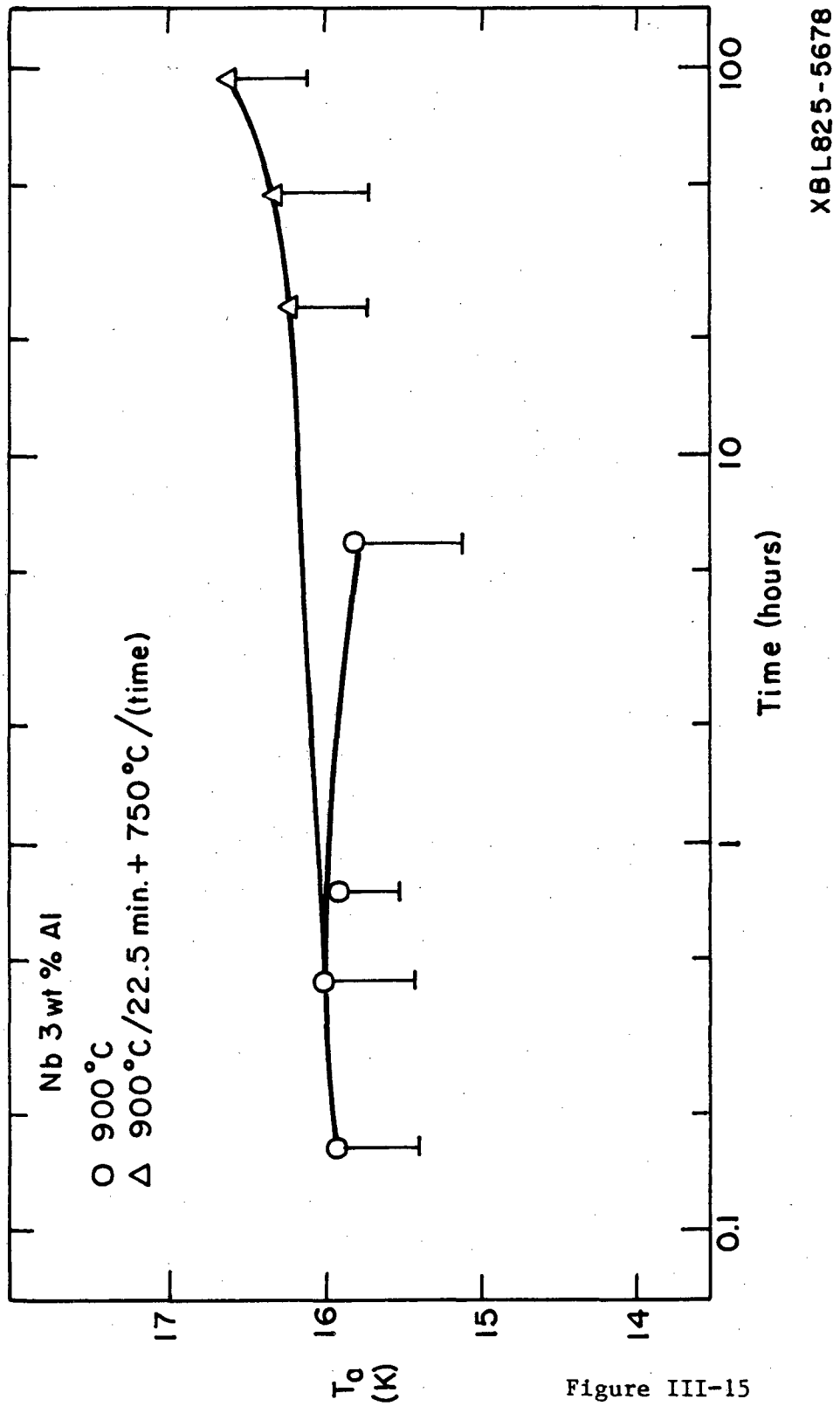

Figure III-15

Figure III-16. Critical temperatures of 3 wt% Al (810422) samples as a function of annealing temperature and time.

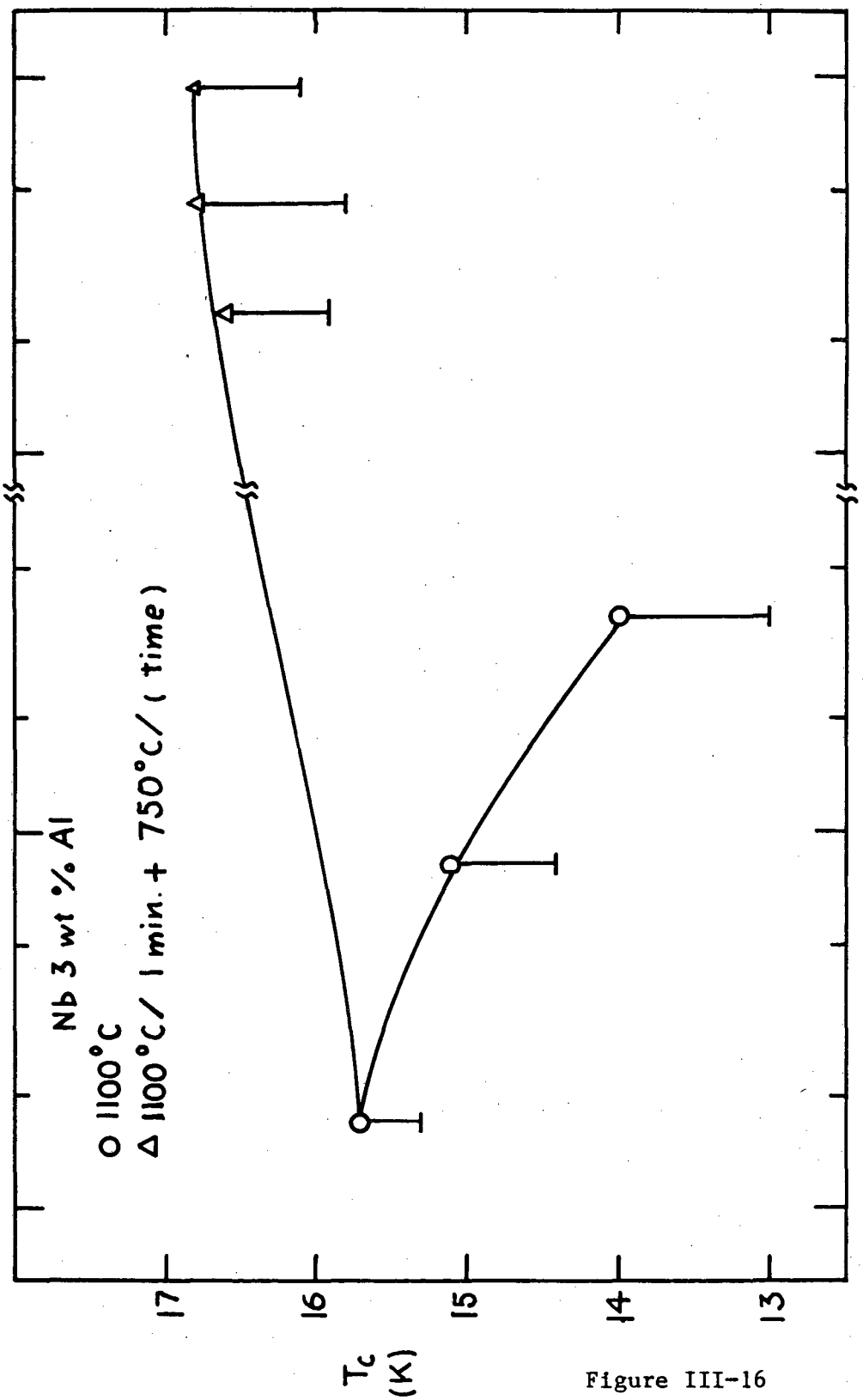

Figure III-16

the P/M processed Nb_3Al wire is fine and complex but has not been clearly characterized yet. Therefore , a thorough correlation between the overall J_c and the heat treatment , in terms of metallurgical characteristics , was unable to be obtained. Preliminary results, however, are interesting and will be presented.

The variation of the overall J_c with the transverse applied magnetic field for samples of number 811027 , given various single-temperature treatments, is shown in Figures III-17 and 18. All of the measurements were performed at 4.2 K . The trend of the overall J_c is similar to that of the T_c onset. If the overall J_c at a particular field were plotted versus the annealing time for a given temperature, the curve would rise slightly upon initial annealing , reach a maximum, and then tend to decrease as the annealing time progressed. For heat treatments performed at 900°C, the maximum occurred around 22.5 minutes. The overall-J_c-vs-applied-magnetic-field-B-curve of a sample given this optimum heat treatment is plotted in Figure III-17 along with that of a sample annealed at the same temperature but for a shorter time (10 minutes). These two curves are represented by open and solid triangles , respectively. At 750°C , the maximum occurred around 2 days. The overall-J_c-vs-B curve of a sample given this heat treatment and that of a sample annealed for a longer time are both plotted in Figure III-18. They are represented by open and solid squares , respectively. At both temperatures , curves for different annealing time are almost parallel to each other at the fields measured. In other words , the optimum of the overall J_c at these high fields for a paticular annealing temperature can be achieved just by finding the optimum time. Other samples seem to exhibit the same trend.

Figure III-17. Overall critical current density of 5 wt% Al (811027) samples as a function of the transverse applied magnetic field.

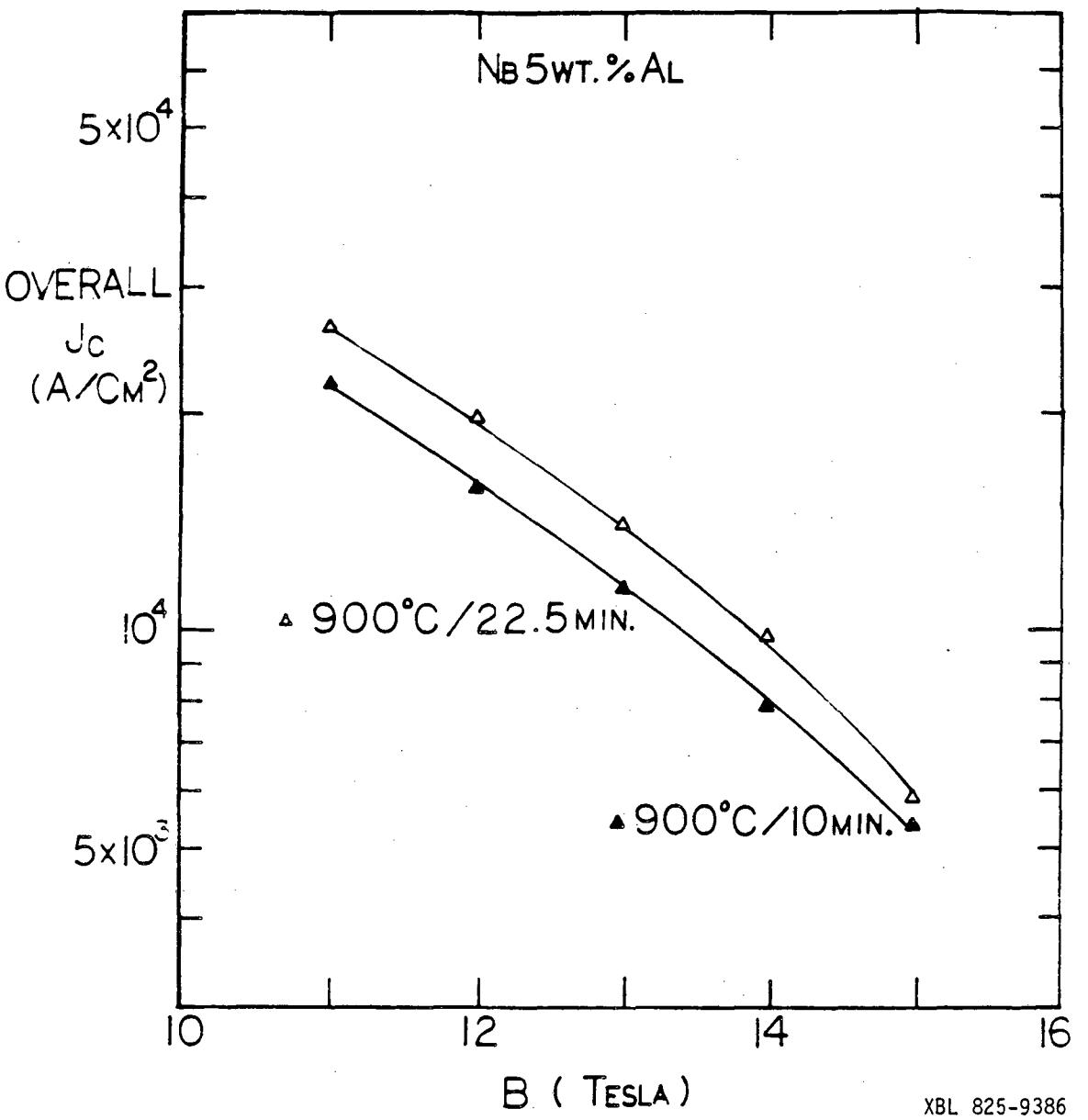

Figure III-17

Figure III-18. Overall critical current density of 5 wt% Al (811027) samples as a function of the transverse applied magnetic field.

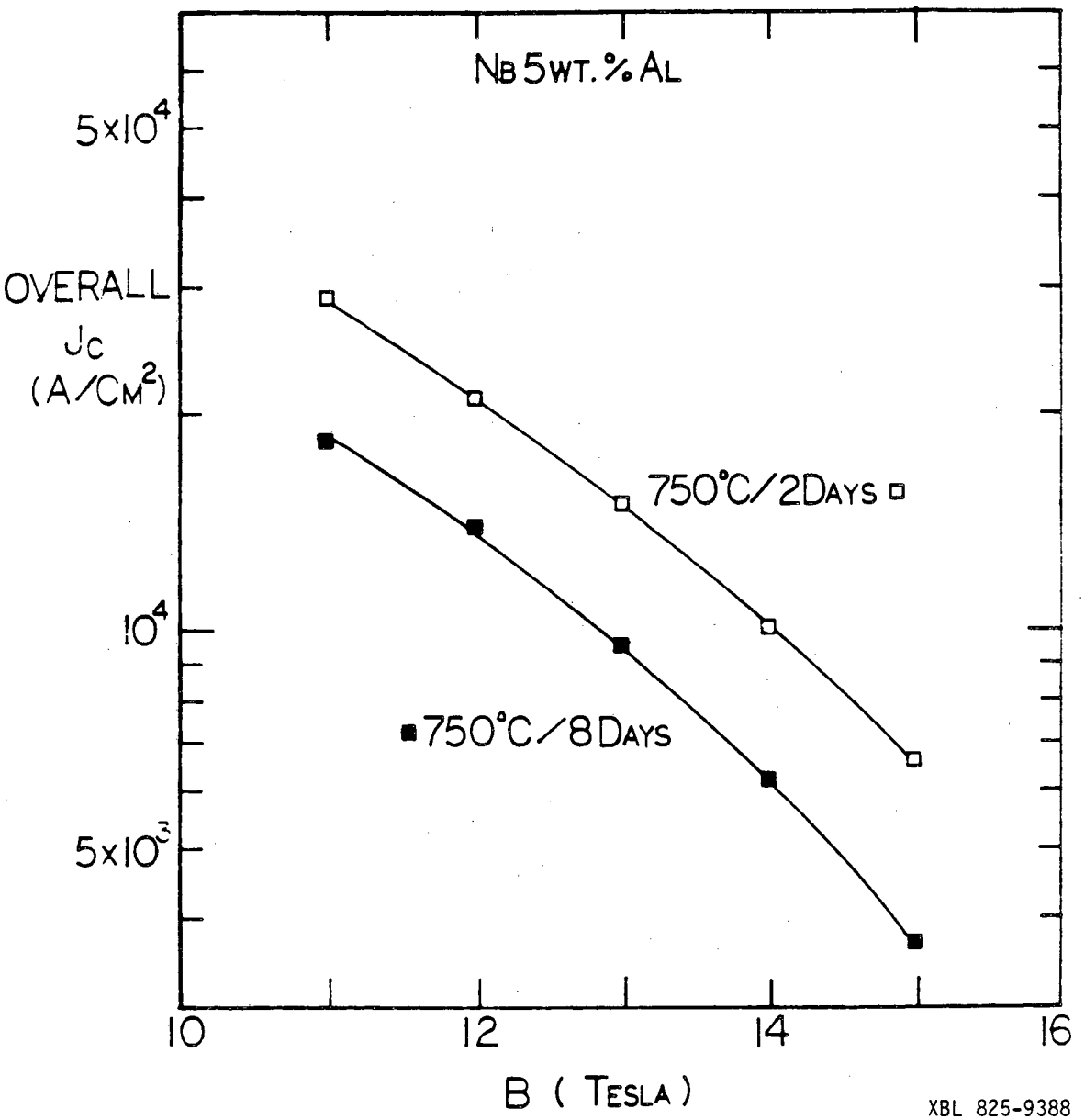

Figure III-18

Double - step treatments can also be employed to improve the overall J_c of the product wire. The results plotted in Figure III-19 indicate that if the optimum heat treatments at different temperatures are combined together , a further increase of the overall J_c at high magnetic fields could be obtained. Represented by open circles is the overall-J_c-vs-B curve of a sample annealed at 900°C for 22.5 minutes plus a subsequent annealing at 750°C for 2 days. Also plotted in the figure is the result of a sample annealed at 900°C for 22.5 minutes only. This is represented by open triangles. With the second annealing at 750°C , the overall J_c at 14 T undergoes an increase of approximately 40% , which is far beyond the estimated 5% error of the measurement. Again, the improvement is evident at all fields measured.

In Figure III-20 , the improvement of the critical current density of samples of 3 wt% Al by double - step treatments is plotted. The overall-J_c-vs-B curves of samples given different heat treatments, namely , 1100°C/1 minute + 750°/2 days , 800°C/12 hours + 700°C/1 day , and 800°C/12 hours are represented by open triangles , circles , and squares, respectively. The results illustrate that a sample treated at 800°C for 12 hours undergoes an increase in critical current at high fields if it is given a subsequent annealing at 700°C for one day. Still better properties are obtained if the sample is given a brief high temperature treatment of 1100°C for 1 minute followed by a more extensive low temperature annealing of 750°C for 2 days. The overall critical current density of this sample as well as that of the double-step-treated sample shown in Figure III-19 has exceeded 10^4 A/cm^2 at 14 T. An even better result is obtained, as plotted in Figure III-21, for a sample of 4 wt% Al, which was given a standard heat treatment of

Figure III-19. Overall critical current density of 5 wt% Al (811027) samples as a function of the transverse applied magnetic field.

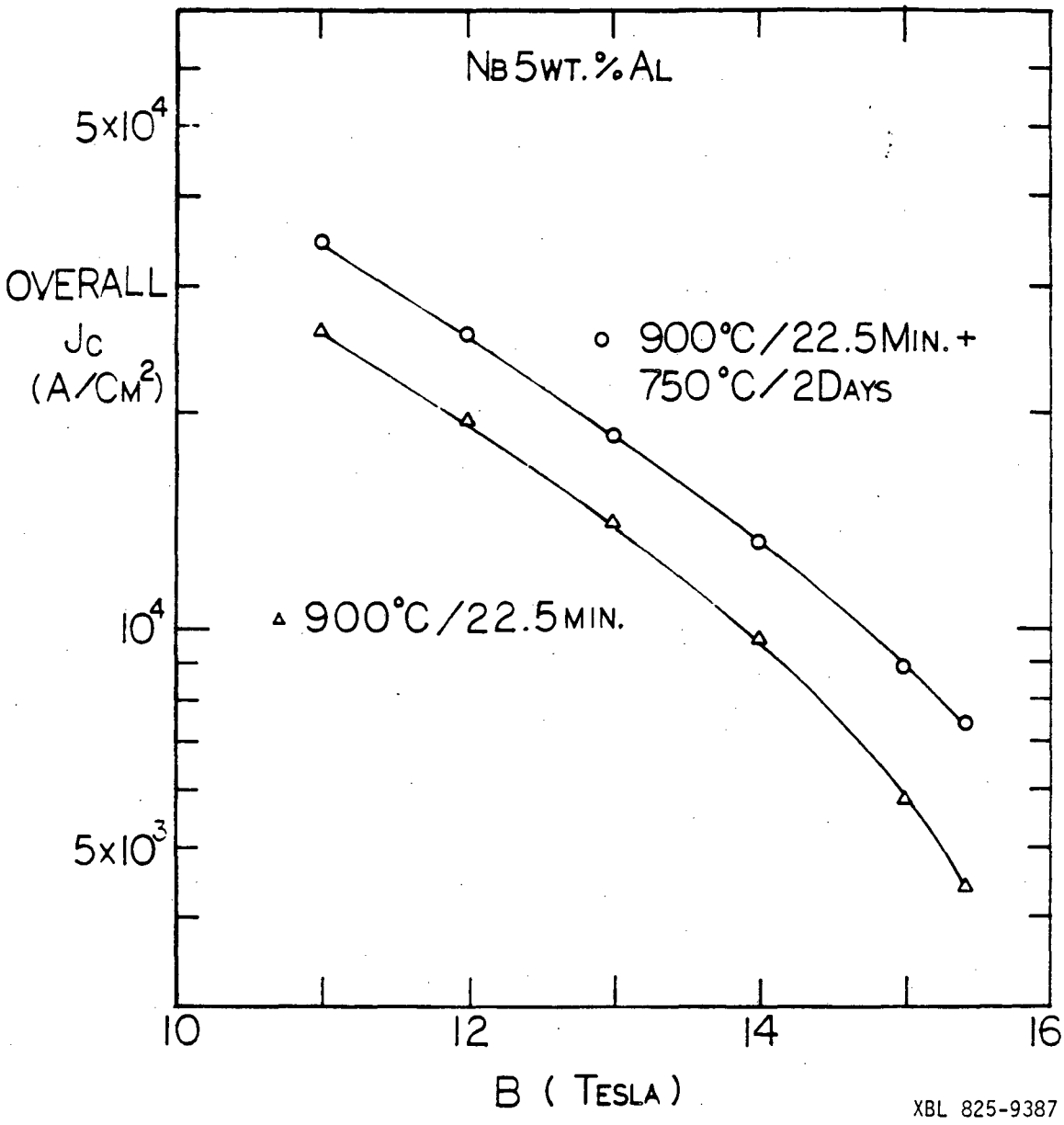

Figure III-19

Figure III-20. Overall critical current density of 3 wt% Al (810422) samples as a function of the transverse applied magnetic field.

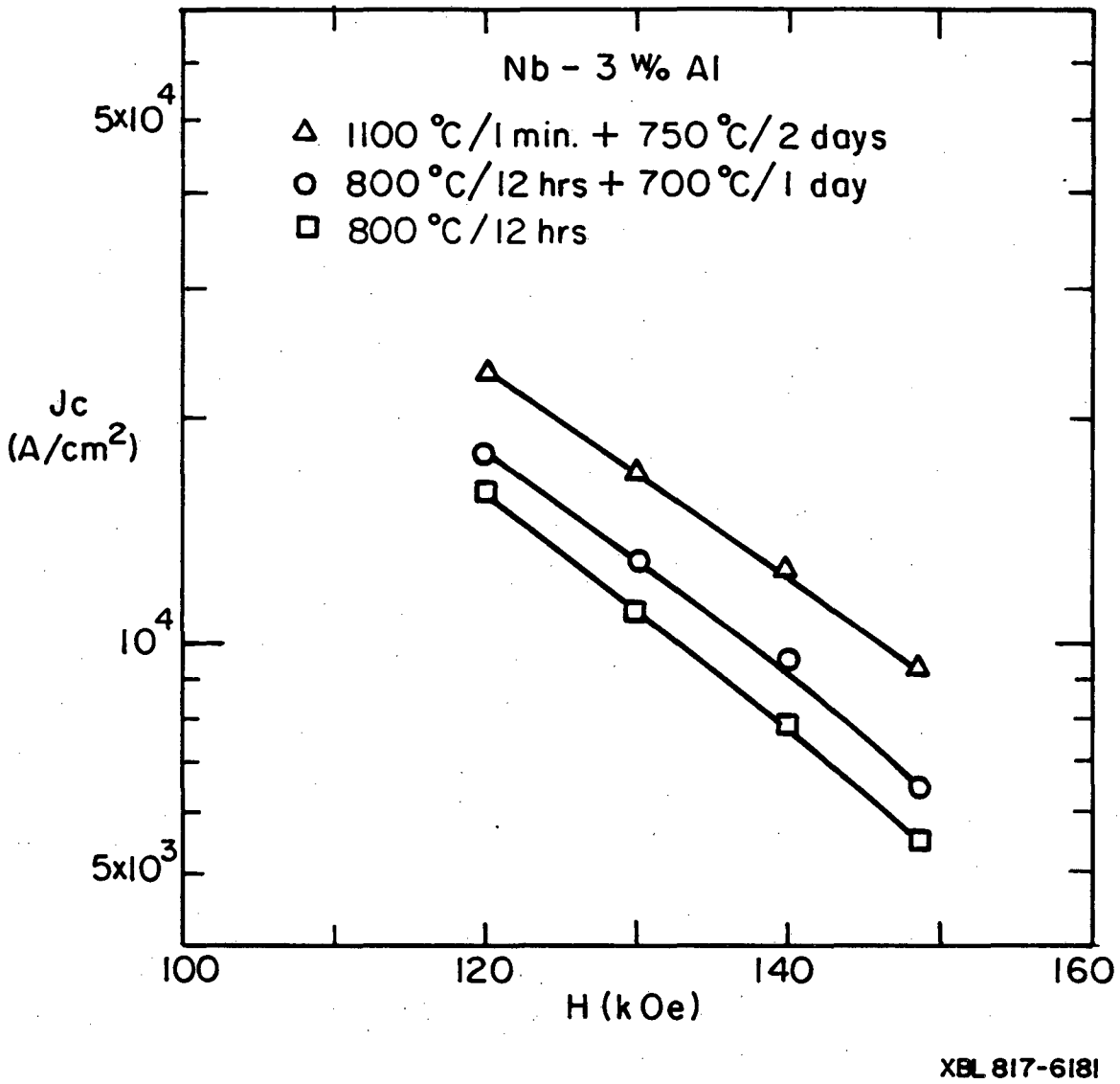

Figure III-20

Figure III-21. Overall critical current density of samples of 3 and 4 wt% Al as a function of the transverse applied magnetic field given a standard heat treatment of 900°C/22.5 minutes + 750/2 days.

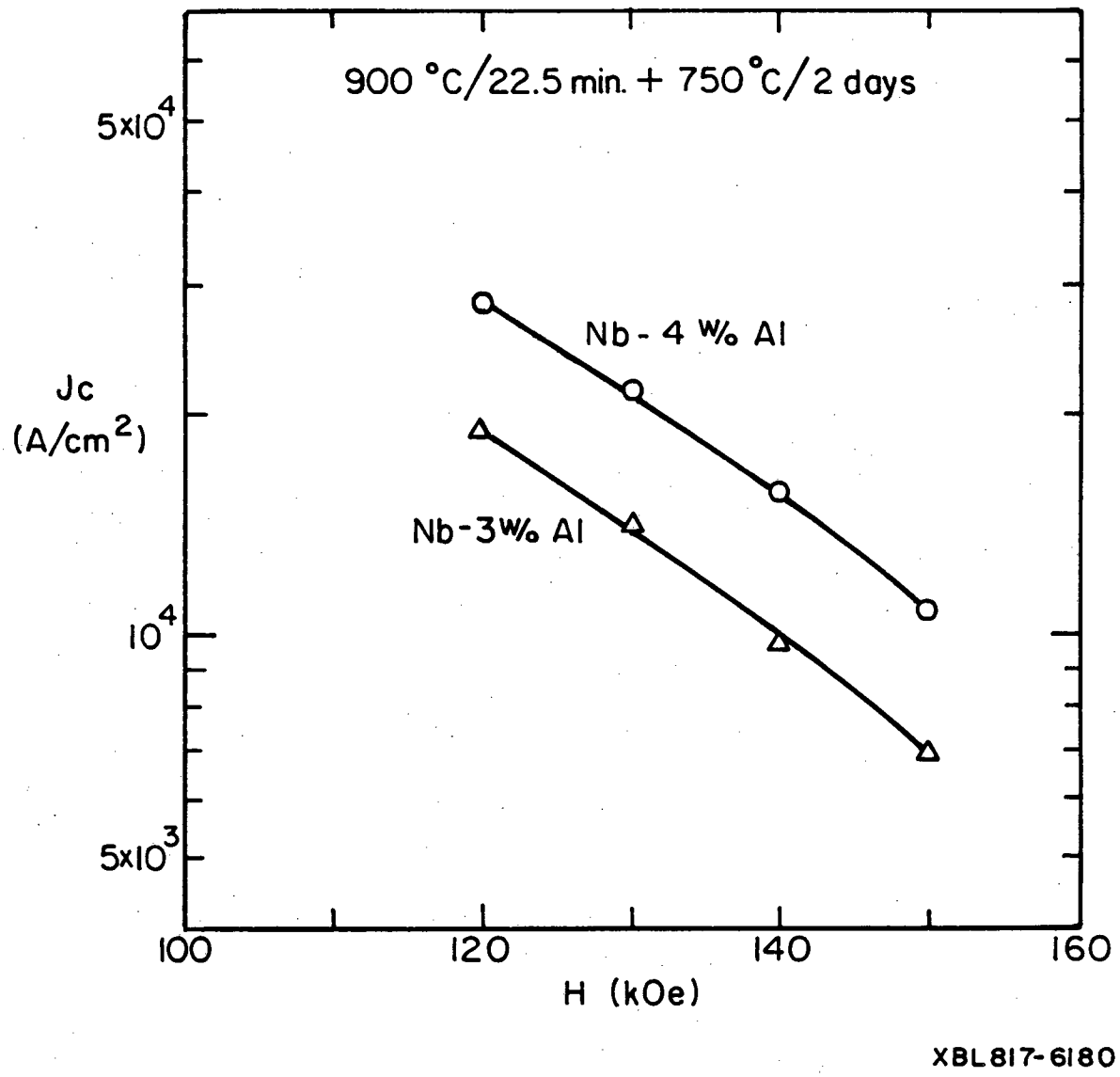

Figure III-21

900°C /22.5 minutes plus 750°C/2 days. The overall J_c is > 10^4 A/cm^2 at 15 T, even though the heat treatment used is not optimal , as can be seen from the results presented in Figure III-20. The critical current is almost tripled when the magnetic field decreases from 15 to 12 T.

If it is tentatively assumed that only the chemical composition and long range order of the superconducting Nb_3Al phase are varied during the second-step annealing , and the variations of all the other factors are negligible, then the behavior of the critical current density with respect to the heat treatment , which is very similar to that of the critical temperature , might be explained by the same reasoning used for the double - step treatments. However, as indicated in the beginning of this section , more extensive studies on the microstructure of the reacted layer with TEM and microanalysis have to be performed if the overall critical current density is to be more closely correlated with the heat treatment.

C. Influence on Overall J_c of Powder Preparation and Deformation Process

Heat treaments can have a large effect on the critical current density of the P/M processed Nb_3Al superconducting wire as described in the last section. Figure III-22 further illustrates this point. In this figure , the best and worst overall J_c values of samples of 5 and 3 wt% Al for all heat treatments performed were picked and plotted against the applied magnetic field. These data points , for each sample , form the upper and lower boundaries of a band in which all other data points fall. The overall-J_c-vs-B bands thus drawn of

Figure III-22. Overall critical current density bands of 5 and 3 wt% Al samples as a function of the transverse applied magnetic field.

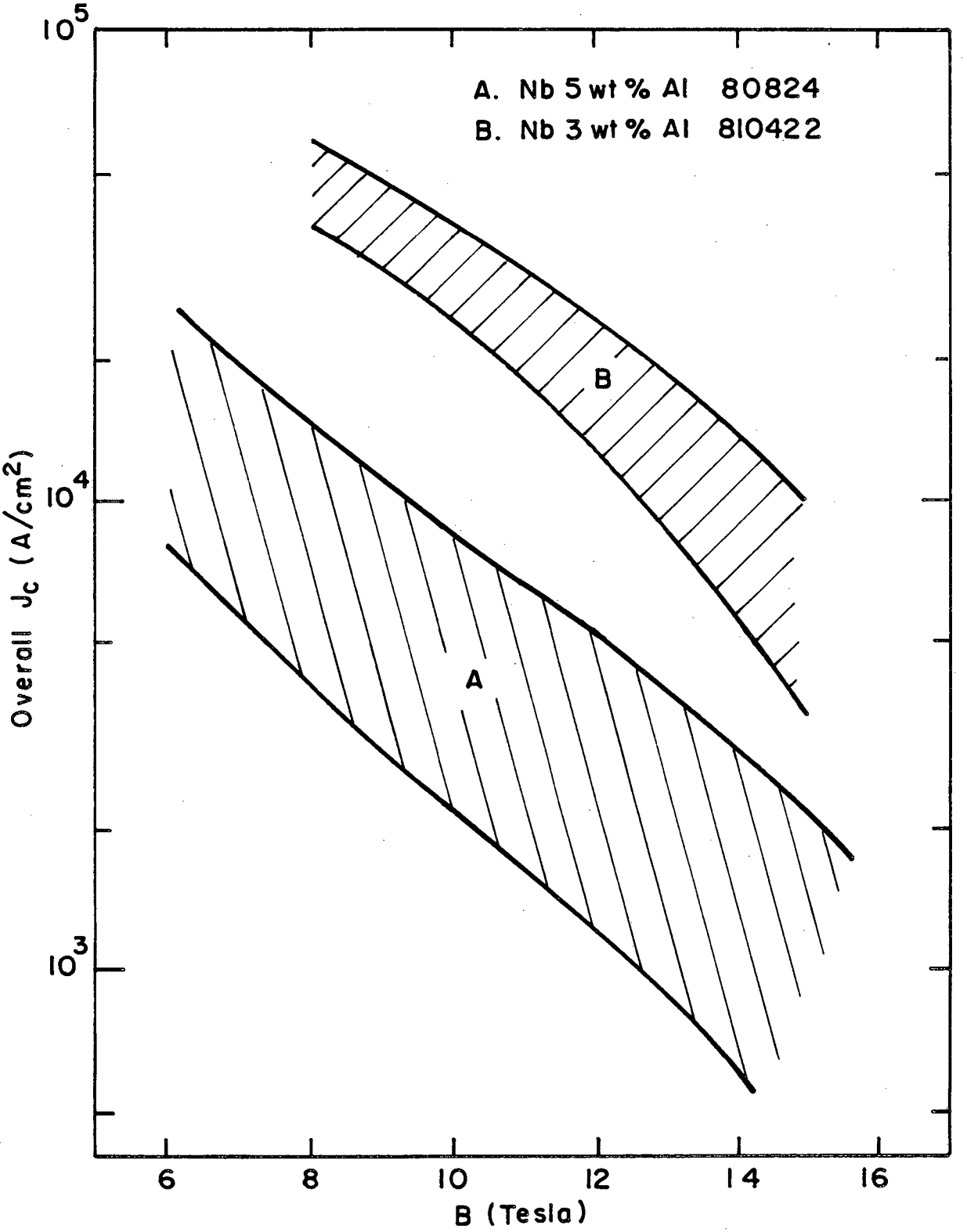

Figure III-22

samples 80824 and 810422 are denoted by "A" and "B", respectively. Band A is the result of the initial run and naturally contains all "good" and "bad" heat treatments. The overall J_c at a particular field can differ by as large as a factor of 4. Band B also includes some "bad" heat treatments but has a smaller width. The critical current can at most differ by a factor of 2.

Though the influence of the heat treatment is large, the optimization of the current- carrying capacity by the heat treatment is limited once the optimum single- temperature treatment is found. Double - step treatments can at most improve the result by a typical value of 40% , if the heat treatments are carefully selected (see Figure III-19 and 20). If, however , other processing parameters are varied, the critical current density could be much improved. For example, in Figure III-22, the best overall J_c of bands A and B differs almost by a factor of 5 at 10 T, even though the latter has a lower Al content. It will be clear later that the superiority of the sample of 3 wt% Al results from the higher reduction and smaller powder sizes employed. It is important , therefore , to study the variation of the current-carrying capacity of the P/M processed binary Nb-Al wire with the processing parameters besides the heat treatment. The results on two of the parameters , namely , the Al content and the areal reduction ratio are presented as follows.

C.1. Al Content

Samples of 4 wt% Al (810608) and 5 wt% Al (811027) were designed metallurgically to achieve an approximately 50 : 50 ratio between the

reaction products (A15 + σ phases) and the residual Nb in the transverse cross section of the product wire. Geometric considerations suggest that , for this purpose , the wire should be made of initial powders having a Nb to Al powder size ratio of approximately 2.7 to 1. These samples were therefore made with approximately this ratio (Table II-1). Their superconducting properties have already been shown in the last few sections.

Akihama et al.[7] used similar powder sizes to those employed in samples of 3 wt% Al (810422) and varied the Al content. They found that 3 wt% Al was an optimum. Our measurements indicate, however, that the overall critical current density of samples of 4 wt% Al could be better if the geometry of the final wire were carefully designed , as illustrated in Figure III-21. The overall J_c of sample of 4 wt% Al showed a significant increase over that of the sample of 3 wt% Al when both samples were given a standard heat treatment of 900°C/22.5 minutes + 750°C/2 days . The improvement of the overall J_c at 14 T , by increasing the wt% Al from 3 to 4, was > 50% . The overall J_c of the latter was above 10^4 A/cm^2 at 15 T and 4.2 K.

A further increase of the Al content from 4 to 5 wt% Al seems to neither improve nor degrade the current-carrying capacity of the product wire. The overall-J_c-vs-B bands of samples of 4 and 5 wt% Al, similar to those shown in Figure III-22 , are plotted in Figure III-23. They are represented by the broken and solid lines , respectively . Overall $J_c > 10^4$ A/cm^2 at 15 T is still readily achieved, but there is no significant difference between these two bands. The reason, however, is unclear for the moment. The trend of the overall critical curent density with Al content > 5 wt% should be further investigated.

Figure III-23. Overall critical current density bands of samples of 5 wt% Al (811027) and 4 wt% Al (810608) as a funtion of the transverse applied magnetic field.

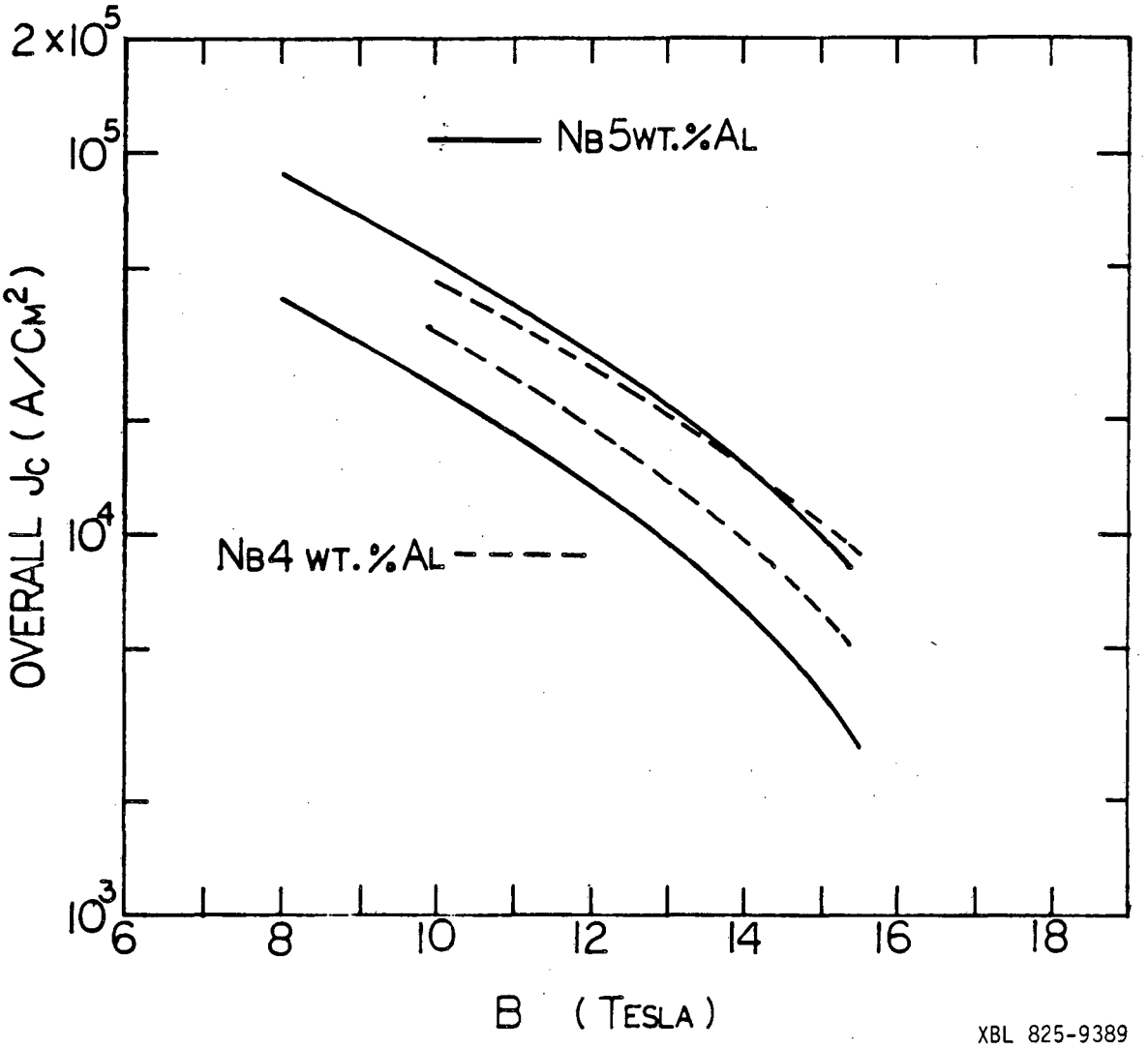

Figure III-23

C.2. Areal Reduction Ratio

The areal reduction ratio R shows a very significant influence on the overall critical current density of the P/M processed Nb_3Al superconducting wire. In Figure III-24 , overall J_c of samples of 5 wt% Al with 5 different reductions is plotted against the applied magnetic field B. These samples were all given an identical heat treatment of 900°C/22.5 minutes. The overall J_c value increases consistently when R is increased from 630 to 880, 1740, 7640, and 17,700. Even for samples with R as high as 7640, the overall J_c still undergoes an increase of ~ 50% at 14 T when R is approximately doubled. The curves are almost parallel to one another at higher fields. At lower fields, those of samples with very high reduction tend to be concave downwards. The effect of the areal reduction ratio can be more clearly presented if the overall critical current density at a particular field is plotted against R , and the result is shown in Figure III-25. The curve on the right , indicated by open circles , is the overall-J_c-vs-R curve of the same samples shown in Figure III-24 in an applied magnetic field of 14 T. It rises sharply at initial reductions but the slope tends to decrease as R is further increased. It is noticed that the curve has not yet reached a plateau even for R as high as 17,700 which corresponds to a reduction of 99.994% in the transverse cross section of the powder wire.

Preliminary x-ray studies of these samples , using a diffractometer, indicate that there is a significant increase of the volume fraction of the A15 phase and a decrease of the σ-phase when the reduction is increased. Two of the spectra are shown in Figure III-26.

Figure III-24. Overall critical current densities of 5 wt% Al samples (811027) of five different reductions as a function of the transverse applied magnetic field.

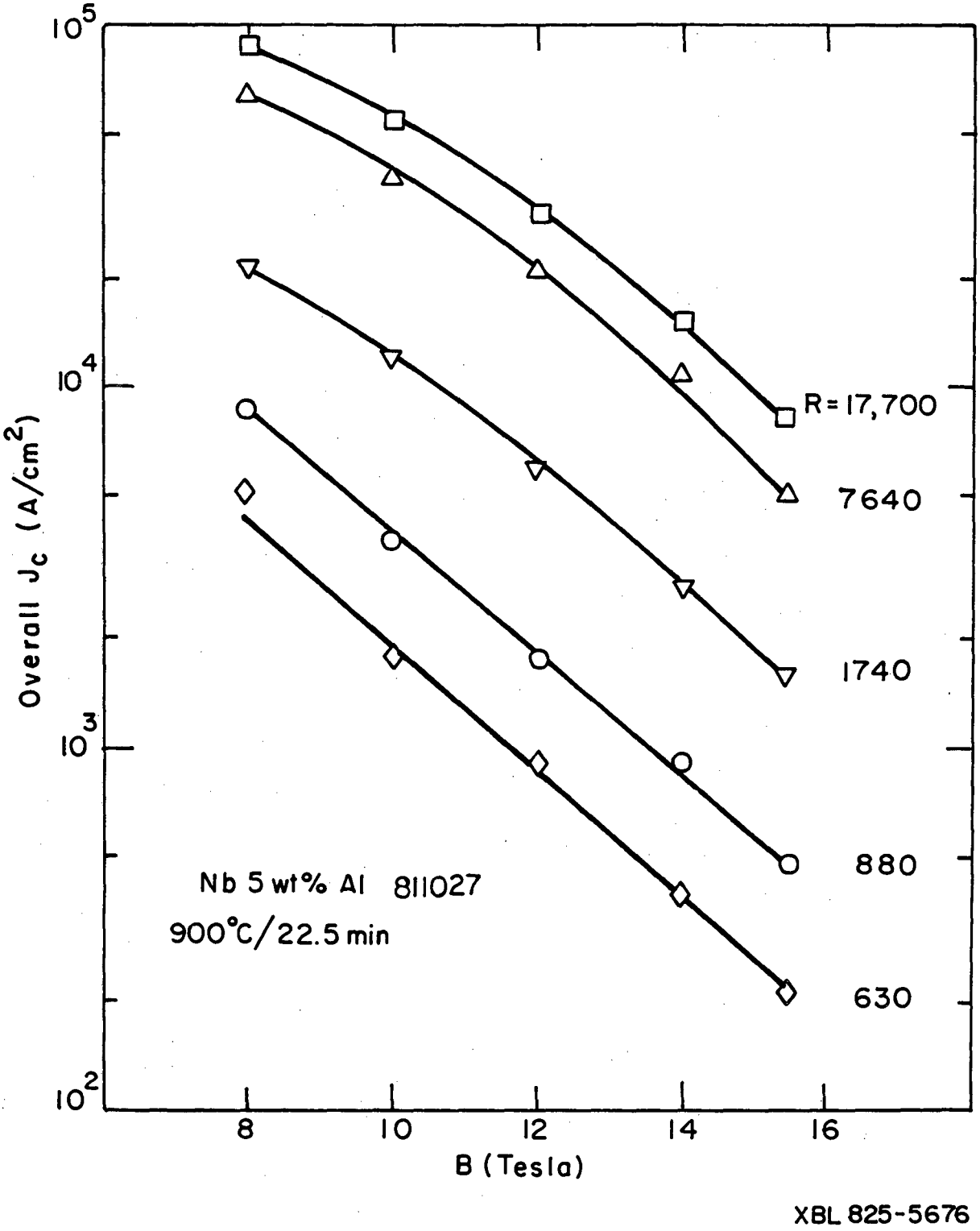

Figure III-24

Figure III-25. Overall current densities at 14 teslas and 4.2 K of samples of 5 and 2.5 wt% Al as a function of the areal reduction ratio.

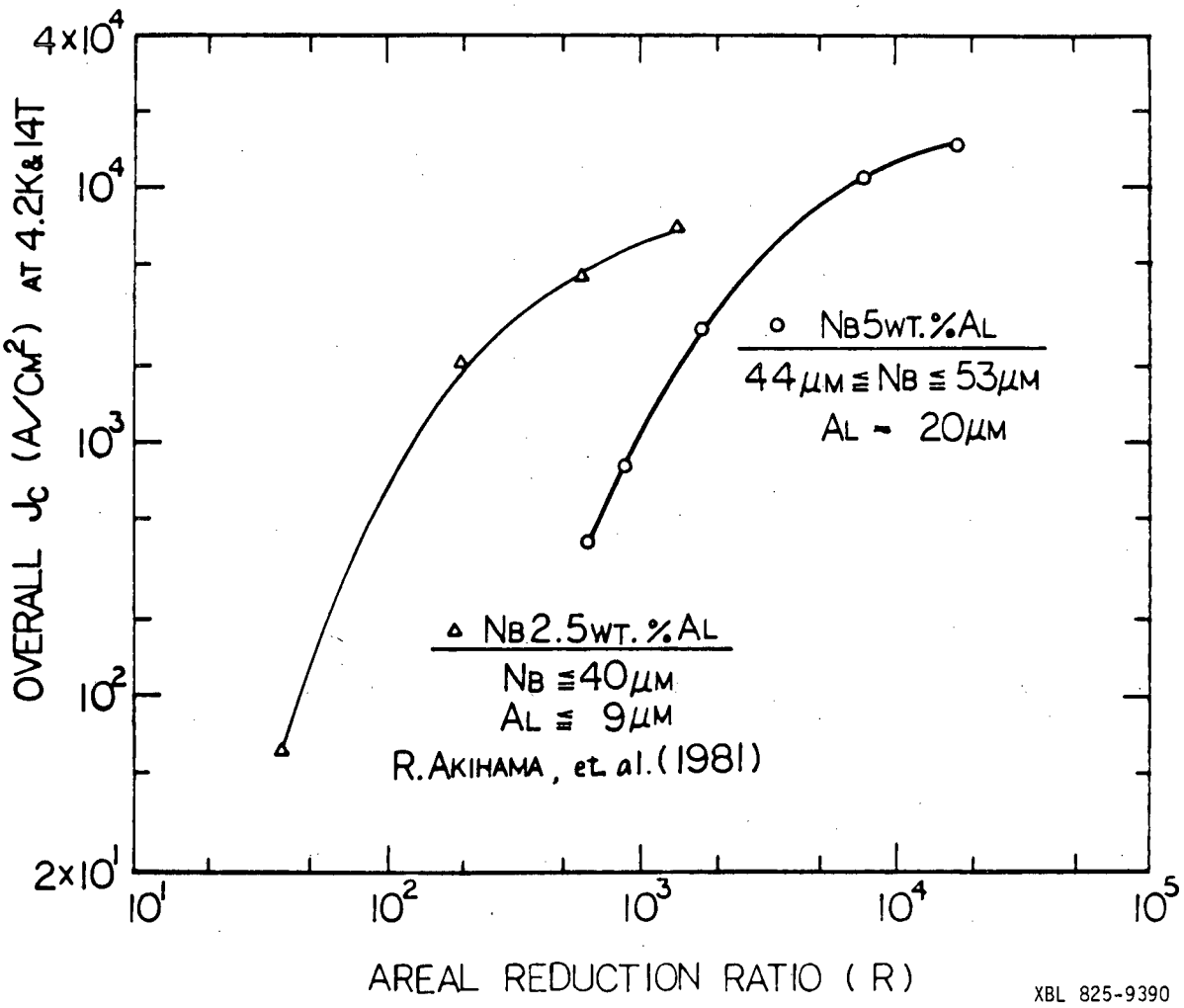

Figure III-25

Figure III-26. Two x-ray spectra of 5 wt% Al samples (811027) of different reductions but of the same heat treatment: 900°C/22.5 minutes. Areal reduction ratios are 1740 and 4660 for the sample in the upper and lower spectra, respectively.

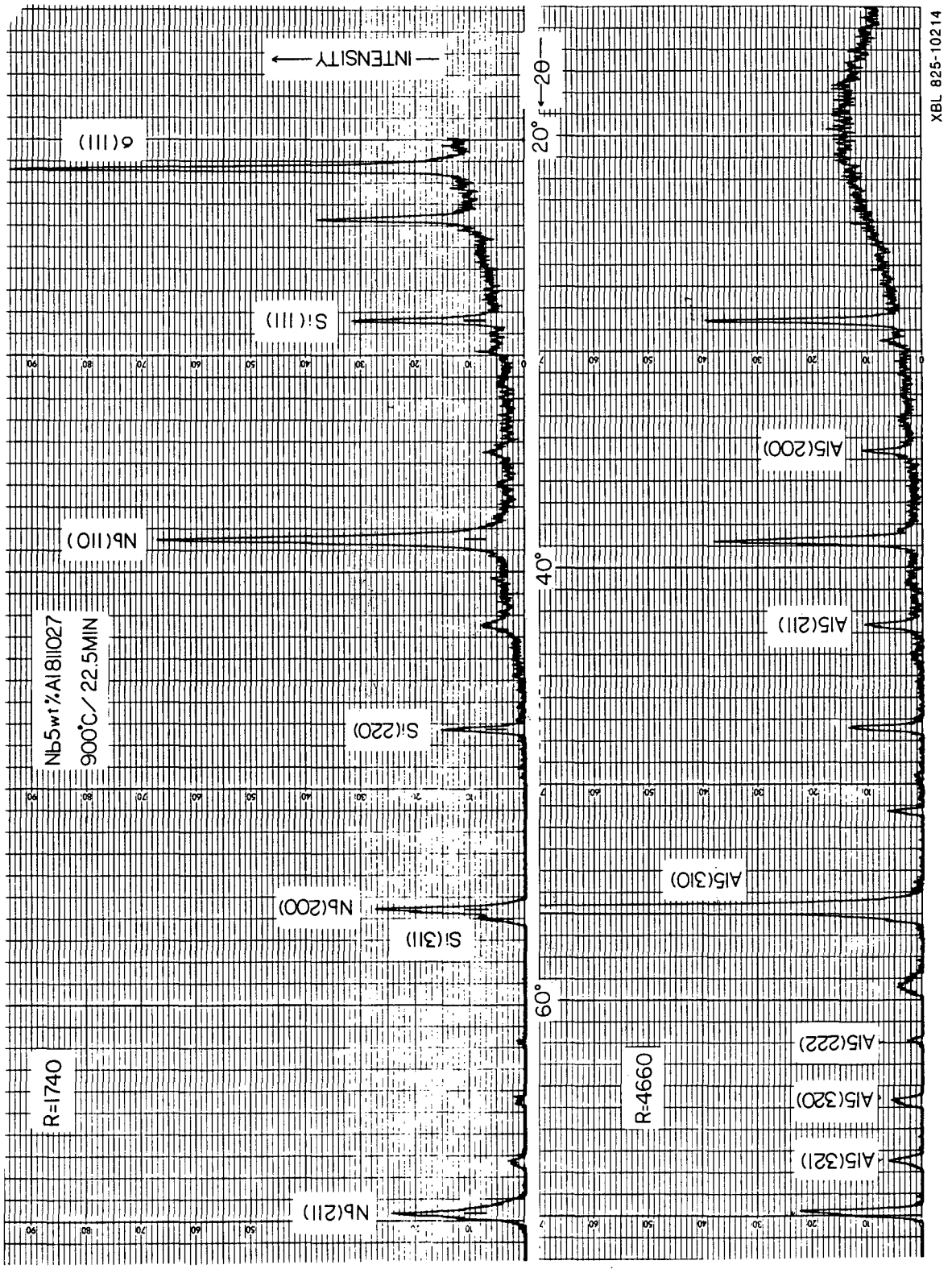

Figure III-26

The x-axis is the 2θ value of the diffraction in degrees and y-axis the intensity in counts. The areal redution ratios are 1740 and 4660 for the upper and lower spectrum, respectively. Silicon standards were incorporated in both scannings and their peak positons in the two spectra are aligned with each other for illustration. Diffraction peaks due to Nb , σ , and Si phases are labeled in the upper spectrum while in the lower spectrum , only those due to the A15 phase are labeled. During the scanning, the sample stage was rotated with a speed > 60 rounds per minute about the normal direction of the flat sample surface. This could eliminate the texture produced by the high deformation process in two of the three dimensions. However, some of the diffraction peaks still exhibit abnormally high intensities, e.g. , those by the σ (111) and A15 (310) in the upper and lower spectrum , respectively. One therefore must be careful in estimating the volume fraction of the phases present. A better way would be to use the spectrum obtained from the Debye- Scherrer camera using powdered samples. The amount of samples needed in employing this method is much smaller than that with a diffractometer. As shown in the figure , for the sample with the higher reduction, the A15 diffraction peaks are clearly visible. The sample with the lower reduction, on the other hand , only reveals small intensites of A15 diffracton peaks. If the abnormally high diffraction peaks are neglected, it is clear that the lower spectrum has a lower Nb to A15 peak-height ratio. For example , after substracting the background contribution, the peak height ratio between two nearby diffraction peaks at low angle, namely, Nb (110) and A15 (200), is ~ 13 to 1 in the upper spectrum. The ratio decreases to ~ 4 to 1 in the lower spectrum. In other words , the volume fraction of the A15 phase is

significantly increased in the sample of higher reduction.

The SEM studies also indicate that more Nb is consumed to form Nb-Al compounds for samples with higher reductions. The transverse and longitudinal cross sections of two samples of R = 880 and 7640, whose critical current densities are shown in Figures III-24 and 25, are presented in the scanning electron micrographs in Figure III-27. Only the Nb phase remains after the chemical etching. The Nb phase of the sample of higher reduction clearly occupies a smaller fracton in both cross sections. It is noticed that the residual Nb filaments of this sample have a much smaller width than those of the sample of lower reduction.

For the moment , neither of the processing parameters discussed, namely, the Al content and areal reduction ratio, is optimized, nor are other parameters , e.g., the powder size ratio. Further study should be performed. In the next section , the relationships between the overall J_c and powder size, R , and Al content from the viewpoint of the reaction will be discussed.

D. Further Discussion

In Figure III-25, two overall J_c-vs-B curves are presented. The curve on the right is that from samples of 5 wt% Al (811027) in this study, while the one on the left shows the results obtained by Akihama et al.[7] Both exhibit a similar variation with the reduction. They rise sharply at small R's and then tend to reach a plateau as R is further increased. The overall J_c curve of the sample of 2.5 wt% Al rises earlier at a smaller reduction and approaches the saturation

Figure III-27. Scanning electron micrographs of 5 wt% Al samples of different reductions but of the same heat treatment: 900°C/22.5 minutes. Areal reduction ratios are 880 and 7640 for samples shown in the upper two and lower two micrographs. Figures (a) and (b) are the transverse cross sections. Figures (a´) and (b´) are the longitudinal cross sections. Figure (a´) has a lower manificaton than the others as indicated by the micron-mark in the figure.

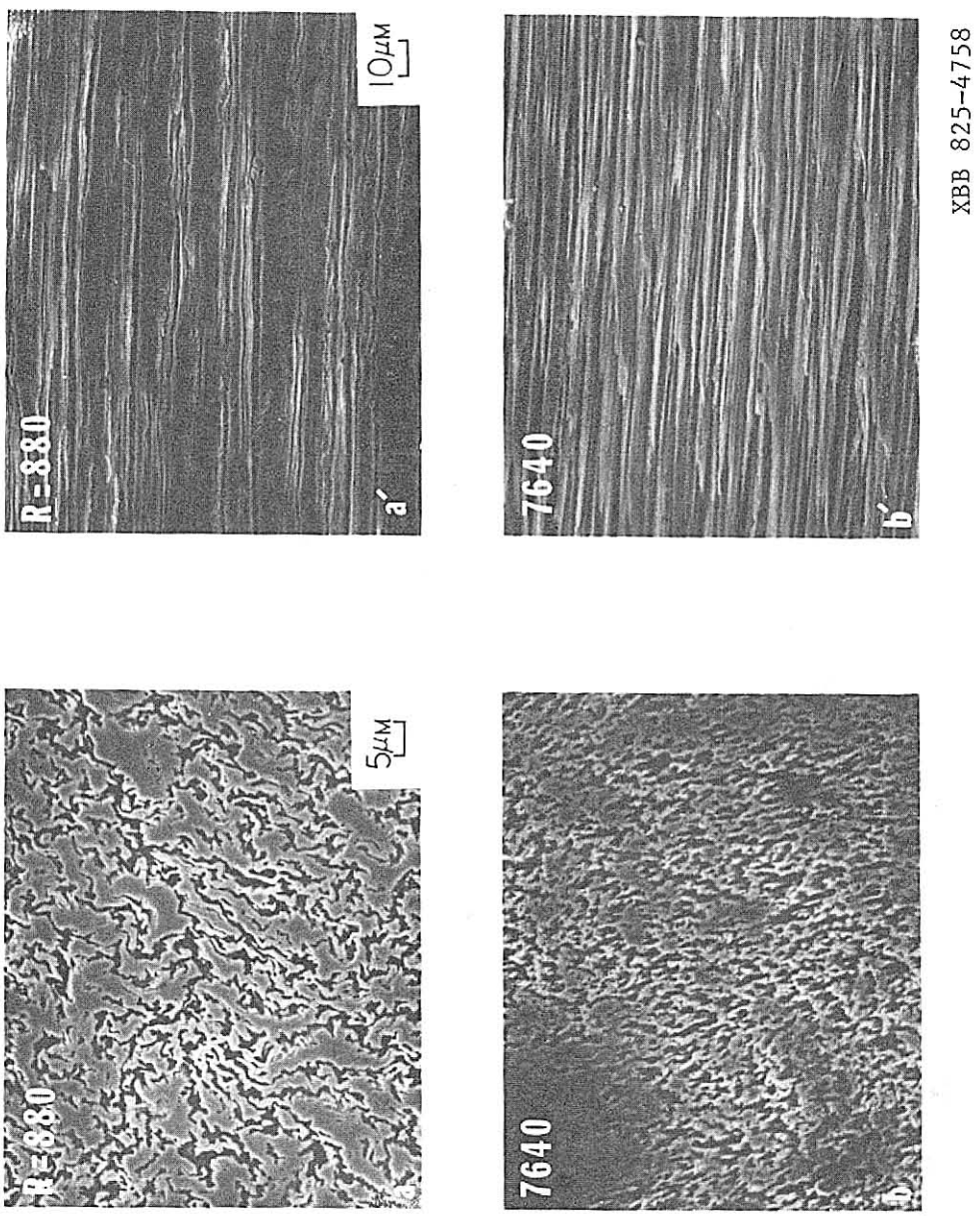

Figure III-27

faster . It reaches 10^3 A/cm^2 when R is just above 10^2 and $\sim 5 \times 10^3$ A/cm^2 when R = 10^3. The overall J_c of the sample of 5 wt% Al reaches 10^3 A/cm^2 when R is $\simeq 10^3$ but exceeds 5×10^3 A/cm^2 if R is only tripled. The plateau of this sample , though not yet reached, seems to be higher than that of the sample on the left; a factor of 2 is estimated. A probable explanation is presented in the following.

Two parameters of the unreacted wire are proposed to investigate how the powder size , powder size ratio , Al content , and R would influence the reaction if these parameters are varied: the thickness t of Al and Nb filaments (or ribbons) and the total area A of the Nb-Al interface. The influence to the reaction by the processing parameters mentioned above will be described in terms of these two parameters.

If only the powder size is different , the wire employing smaller powders would have a larger Nb-Al interfacial area. The thickness of the filaments , on the other hand, would be smaller . During the reaction, therefore , there would be more chance for Al to react with Nb and , at the same time , the diffusion distance would be smaller . The total time needed to transform all of the Al in the wire into A15 compounds would thus be shorter. This would result in the formation of the same amount of A15 compounds but with smaller grain sizes since A15 grains would grow with the reaction time. It is generally believed that A15 grain boundaries are the main flux pinning centers in the A15 superconducting wire.[8-16] Hence, the wire employing smaller powders would carry a higher critical current if every other parameter remains the same. This reasoning seems to be in accordance with the result obtained by Annaratone et al.[17] The critical current of their "jelly-roll"-processed Nb_3Al wire decreases linearly with the thickness of the

Al foil used. The Overall J_c differs by an order of magnitude when the Al foil thickness is only decreased by a factor of ~4.

If the ratio between powder size or the Al content is varied , the A value would also change. The closer the ratio is to 1 , the larger the A value would be. One should be careful when considering the optimal ratio , however , since Nb and Al powders have a different deformability. After the deformation , the ratio between Nb and Al filament thickness would thus be different from that between the initial powder sizes. The increase of Al content would also result in an increase of the volume fraction of the A15 phase in the product wire.

If the areal reduction ratio R is increased , t would decrease. The total time needed to consume all of the Al would also decrease as dicussed above. This conclusion is supported by the fact that, for the same annealing temperature and time, samples of higher R's have a higher volume fraction of A15 phase (see Figure III-26 and the discussion in the last section). As a result, the overall J_c is higher for these samples.

Looking into Figure III-25 again, one could now explain the phenomena based on the reasoning presented above. The sample of 2.5 wt% Al employs a much wider range of initial powder size , which extends from very small values up to 40 and 9 μm for Nb and Al, respectively . The average sizes are most probably around 20 and 5 μm . These are rather small as compared to those of the powders used in fabricating samples of 5 wt% Al, which have an average powder size of approximately 50 and 20 μm for Nb and Al , respectively. Therefore, samples of 5 wt% Al needs a larger reduction to achieve the same filament dimension as that of the samples of 2.5 wt% Al. Consequently, the overall J_c curve

of the former lies to the right of the curve of the latter . Yet because of higher Al content , samples of 5 wt% Al could have a higher volume fraction of A15 compounds and thus could reach a higher overall J_c after sufficient reductions. The extra effort made in achieving a higher reduction is compensated by the better quality of the wire fabricated. Meters of wires of uniform cross sections could be drawn, where the length of the wire was only limited by the facility available. The sample of 2.5 wt% Al , on the other hand , suffered severe difficulties when deforming and was not readily produced in long lengths.[18] It is interesting to note that samples of 3 wt% Al (810422), which employed similar ranges of the powder dimension as those of the sample of 2.5 wt% Al, could be deformed to an R of ~1600 and be produced in meters length without great difficulties. One possible factor that might contribute to the difference in deformability of these two wires is that the powders employed to fabricate samples of 3 wt% Al were passed through a micro- classifier to remove very fine particles. It is known that smaller powders have higher microhardness values, presumably because these powders have a higher impurity content, e.g., oxygen. They are therefore more difficult to deforme.

CHAPTER IV. CONCLUSIONS

The possibility of obtaining very promising values of the critical temperature and high - field critical current density in powder-metallurgy- processed Nb_3Al superconducting wires was demonstrated in this thesis work. Inductive T_c onset of 17 K with a superconducting-to-normal transition width of < 1 K and overall J_c of > 10^4 A/cm^2 at 15 teslas and 4.2 K were achieved. Double-step treatments, beginning with heat treatments at high temperatures followed by annealings at lower temperatures , were shown to be beneficial to both T_c and overall J_c. An increase of the Al content from 3 to 4 wt% Al, with metallurgical considerations on the microstructure within the product wire, resulted in an increase of the critical current density. A further increase of 1 wt% Al seemed to neither improve nor degrade the critical current density. The reduction in the transverse cross section of the powder wire was found to play an important role in determining the overall J_c. Overall J_c of 5 wt% Al (81102) samples was found to be a monotonically increasing function of the areal reduction ratio R and did not reach a plateau even for R as high as 17,700 . Samples employing smaller powder sizes demonstrated a good overall J_c value at a smaller R than those employing larger powder sizes. The latter, however, had a better deformability. The results suggest the importance of the Nb and Al filament thickness and the total Nb-Al interfacial area of the powder wire in determining the peak current a Nb_3Al superconducting wire can transport.

Microstructural analysis of the reacted samples revealed a fine, complex microstructure. In the initial reaction , four phases were

found: the residual Nb , the Nb_3Al (A15) , Nb_2Al (σ) and $NbAl_3$. As annealing time progressed, the $NbAl_3$ phase was consumed , but two competing phases, namely, the A15 and σ-phases, remained along with the residual Nb. Preliminary x-ray studies using a diffractometer indicated that a sample of higher reduction can have a higher volume fraction of the A15 phase than that of a lower reduction sample given an identical standard heat treatment. This was further supported by a SEM analysis on both transverse and longitudinal cross sections of the two samples.

The powder metallurgy process is a simple , straightforward , and yet flexible process. The powder sizes , powder size ratio(s) , and chemical composition can be varied easily. With suitable cladding materials, areal reduction ratio as high as 17,700 can be achieved using the laboratory facilities available , which corresponds to a reduction of 99.994% in the transverse cross section. With the facilities available in industrial practice, much higher reductions can be expected.

The results reported here suggest that much better properties are obtainable in the powder-metallurgy-processed A15 Nb_3Al superconducting wire. The further clarification of the microstructures should permit a choice of powder characteristics, wire processing, and heat treatment conditions leading to superior superconducting characteristics. To be employed as practical superconductors, the research on both the mechanical properties and the AC loss of the powder wire should also be performed.

V. REFERENCES

Chapter I.

1. K. Tachikawa and Y. Tanaka, Japan J. Appl. Phys. 5, 834 (1966).
2. A. R. Kaufman and J.J. Pickett, Bull. Am. Phys. Soc. 15, 838 (1970)
3. C.C. Tsuei, J. Appl. Phys. 45, 1385 (1974).
4. S. Foner, R. Roberge, J. L. Fihey, R. Flükiger , R. Akihama , E. J. McNiff, Jr., and B. B. Schwartz, 8th Symposium on Eng. Problems of Fusion Research, Nov. 13-16, 1979, San Francisco, California.
5. J. D. Verhoven , E. D. Gibson, C. V. Owen, J.E. Ostenson, and D. K. Finnermore, Appl. Phys. Lett. 35, 270 (1979).
6. R. Roberge, S. Foner, E. J. McNiff, Jr., B. B. Schwartz, and J. L. Fihey, IEEE Trans. Magn. MAG-15, 687 (1979).
7. K. Tachikawa, Cryogenics 19, 307 (1979).
8. J. Bevk , F. Habbal , C. J. Lobb , and J. P. Harbison , Appl. Phys. Lett. 35, 93 (1979).
9. T. Luhman , "Treatise on Materials Science and Technology", Vol.14, ed. T. Luhman and D. Dew-Hughes, p.224 , Academic, New York (1979); and the references therein.
10. J. M. Hong , I. W. Wu , J. T. Holthuis , M. Hong, and J. W. Morris, Jr., to be published in Advances in Cryogenic Engineering, Vol.28, Plenum Press, New York (1981).
11. R. Akihama, R. J. Murphy, and S. Foner, Appl. Phys. Lett. 37, 1107 (1980).
12. R. Flükiger , R. Akihama , S. Foner , E. J. McNiff , Jr., and B. B. Schwartz, Appl. Phys. Lett. 35, 810 (1979); and earlier references

therein.

13. R. Borman, H. C. Freyhardt, and H. Bergmann, Appl. Phys. Lett. 35, 944 (1979).

14. B. Annaratone , R. Bruzzese , S. Ceresara , V. Pericoli-Ridolfini, G. Pitto, and N. Sacchetti, IEEE Trans. Magn. MAG-17, 1000 (1981); and earlier references therein.

15. S.S. Shen and W. K. McDonald , to be published in Advances in Cryogenic Engineering, Vol.28, Plenum Press, New York (1981).

16. M. R, Pickus, J. T. Holthuis, and M. Rosen, "Filamentary A15 Superconductors" ed. M. Suenaga and A. F. Clark, p.331, Plenum Press, New York (1981); and references therein.

17. M. Hong , D. Dietderich, and J. W. Morris, Jr., J. Appl. Phys. 51, 2774 (1980).

18. M. Hong and J. W. Morris, Jr., Appl. Phys. Lett. 37, 1044 (1980).

19. E. A. Wood, V. B. Compton, B. T. Matthias , and E. Corenzwit, Acta Crystallogr. 11, 604 (1958).

20. E. Corenzwit, J. Phys. Chem. Solids 9, 93 (1959).

21. R. H. Willens, T. H. Geballe, A. C. Gossard, J. P. Matia, A. Menth, G. W. Hull, Jr., and R. R. Soden, Solid State Commun. 7, 837 (1969)

22. S. Foner , E. J. McNiff , Jr. , T. H. Geballe , R. H. Willens , E. Buehler, Physica 55, 534 (1971).

23. G. W. Webb , Appl. Phys. Lett. 32, 773 (1978) ; IEEE Trans. Magn. MAG-15, 616 (1979).

24. J. A. Woollam, S. A. Alterovitz, E. Haugland, and G. W. Webb, Appl. Phys. Lett. 36, 706 (1980).

25. C. E. Lundin and A. S. Yamamoto, Trans. Met. Soc. AIME 236, 863 (1966).

26. V. N. Svechnikov, V. M. Pan, and V. I. Latysheva, Metallofizika 32, 28 (1970).

27. J. L. Jorda , R. Flükiger , A. Junod , and J. Müller, IEEE Trans. Magn. MAG-17, 557 (1981).

28. A. Junod , J. L. Staudenmann , J. Müller , and P. Spitzli, J. Low Temp. Phys. 5, 25 (1971).

29. E. Ehrenfreund , A. C. Gossard, and J. H. Wernick, Phys. Rev. B4, 2906 (1971).

30. See the review article by M. Weger and J. B. Goldberg, Solid State Phys. 28, 1 (1973).

31. J. Kwo and T. H. Geballe, Phys. Rev. B23, 3230 (1981).

32. J. Kwo , T. P. Orlando , and M. R. Beasley , Phys. Rev. B24, 2506 (1981).

33. A. Isao , T. Noguchi , Y. Uchida , and A. Kono, J. Vac. Sci. and Technol. 7, 557 (1970).

34. J. G. Kohr, B. P. Strauss, and R. M. Rose, IEEE NS-18, 716 (1971).

35. J. G. Kohr , T. W. Eager , and R. M. Rose, Met. Trans. 3, 1177 (1972).

36. R. Löhberg, T. W. Eager, I. M. Puffer, and R. M. Rose, Appl. Phys. Lett. 22, 69 (1973).

37. D. E. Harasyn and L. E. Toth, J. Appl. Phys. 46, 2232 (1975).

Chapter II.

1. Supplied by Teledyne Wah Chang, Albany, Oregon.

2. Fabricated by W. S. Tyler Incorporated/Screening Division, Ohio.

3. By Harry W. Dietert Co., Michigan.

4. R. Flükiger, S. Foner, E. J. McNiff, Jr., and B. B. Schwartz, Appl. Phys. Lett. 34, 763 (1979); and related references therein.

5. R. Flükiger, S. Foner, E. J. McNiff, Jr., B. B. Schwartz, J. Adams, S. Forman, T. W. Eager, and R. M. Rose, IEEE Trans. Magn. MAG-15, 689 (1979).

6. The chemical composition of Monel 400 : 66% Ni + Co , 31.5% Cu, 1.35%Fe, 0.90% Mn, 0.15% Si, 0.12% C and very few S.

7. D. E. Harasyn and L.E. Toth, J. Appl. Phys. 46, 2232 (1975).

8. J. H. N. van Vucht , H. A. C. M. Bruning , H.C. Donkersloot , and A. H. Gomes de Mesquita, Phllips Res. Rep. 19, 407 (1964).

Chapter III.

1. L. V. Azåroff, "Elements of X-Ray Crystallography", p.535, McGrall-Hill, (1968).

2. Etching in a solution of HNo_3 (70%) : HF (48%) : H_2O = 5 : 1 : 10 for 2 minutes at room temperature.

3. C. E. Lundin and A. S. Yamamoto , Trans. Met. Soc. AIME 236, 863 (1966).

4. J. L. Jorda , R. Flükiger , A. Junod , and J, Müller, IEEE Trans. Magn. MAG-17, 557 (1981).

5. J. Kwo, R. H. Hammond, and T. H. Geballe, J. Appl. Phys. 51, 1726 (1980).

6. D. Dew-Hughes, "Treatise on Materials Science and Technology" Vol.14, ed. T. Luhman and D. Dew-Hughes, p.156 , Academic Press (1979); and the references therin.

7. R. Akihama, R. J. Murphy, and S. Foner, IEEE Trans. Magn. MAG-17,

274 (1981).

8. J. S. Caslaw, Cryogenics 11, 57 (1971).
9. R. M. Scanlan , W. A. Fietz , and E. F. Koch , J. Appl. Phys. 46, 2244 (1975).
10. T. Luhman, C. S. Pande, and D. Dew-Hughes, J. Appl. Phys. 47, 1459 (1976).
11. B. J. Shaw, J. Appl. Phys. 47, 2143 (1976).
12. R. E. Howard , M. R. Beasley , T. H. Geballe , C. N. King , R. H. Hammond, R. H. Norton, J. R. Salem, and R. B. Zubeck, IEEE Trans. Magn. MAG-13, 138 (1977).
13. A. W. West and R. D. Rawlings, J. Mat. Sci. 12, 1862 (1977).
14. J. D. Livingston, Phys. Stat. Sol. (a) 44, 295 (1977).
15. J. Bevk and J. P. Harbison, J. Mat. Sci. 14, 1457 (1979).
16. M. Hong and J. W. Morris, Jr., Appl. Phys. Lett. 37, 1044 (1980).
17. B. Annaratone , R. Bruzzese , S. Ceresara , V. Pericoli-Ridolfini, G. Pitto, and N. Sacchetti, IEEE Trans. Magn. MAG-17, 1000 (1981).
18. S. Foner, private communication.

TECHNICAL INFORMATION DEPARTMENT
LAWRENCE BERKELEY LABORATORY
UNIVERSITY OF CALIFORNIA
BERKELEY, CALIFORNIA 94720